GENE EDITING

In vivo editing of lung stem cells for durable gene correction in mice

Yehui Sun[1]†, Sumanta Chatterjee[1]†, Xizhen Lian[1], Zachary Traylor[2], Sandhya R. Sattiraju[3], Yufen Xiao[1], Sean A. Dilliard[1], Yun-Chieh Sung[1], Minjeong Kim[1], Sang M. Lee[1], Stephen Moore[1], Xu Wang[1], Di Zhang[1], Shiying Wu[1], Pratima Basak[1], Jialu Wang[3], Jing Liu[3], Rachel J. Mann[2], David F. LePage[2], Weihong Jiang[2], Shadaan Abid[4], Mirko Hennig[3], Anna Martinez[3], Brandon A. Wustman[3], David J. Lockhart[3], Raksha Jain[4], Ronald A. Conlon[2], Mitchell L. Drumm[2], Craig A. Hodges[2], Daniel J. Siegwart[1]*

In vivo genome correction holds promise for generating durable disease cures; yet, effective stem cell editing remains challenging. In this work, we demonstrate that optimized lung-targeting lipid nanoparticles (LNPs) enable high levels of genome editing in stem cells, yielding durable responses. Intravenously administered gene-editing LNPs in activatable tdTomato mice achieved >70% lung stem cell editing, sustaining tdTomato expression in >80% of lung epithelial cells for 660 days. Addressing cystic fibrosis (CF), NG-ABE8e messenger RNA (mRNA)–sgR553X LNPs mediated >95% cystic fibrosis transmembrane conductance regulator (CFTR) DNA correction, restored CFTR function in primary patient-derived bronchial epithelial cells equivalent to Trikafta for F508del, corrected intestinal organoids and corrected R553X nonsense mutations in 50% of lung stem cells in CF mice. These findings introduce LNP-enabled tissue stem cell editing for disease-modifying genome correction.

Gene editing is anticipated to revolutionize the field of medicine by creating durable therapies across a wide spectrum of diseases (*1*, *2*). Direct delivery of gene editors to target cells using synthetic nanoparticle- or virus-based systems could facilitate efficient and precise gene editing directly within the patient's body, bypassing the complexities, risks, and costs associated with ex vivo procedures (*3*–*5*). Although progress has been made targeting differentiated cells, such as hepatocytes (*6*) and T cells (*7*), nanoparticle delivery of gene editors to stem cells in vivo has remained elusive. Achieving durable therapeutic responses likely requires editing in tissue-resident stem cells to overcome the loss of corrected DNA in differentiated cells that regularly turn over (*2*, *8*).

Genetic lung diseases constitute a large unmet medical need (*9*, *10*) that could be addressed by corrective strategies if major delivery challenges were overcome. Effective delivery vehicles must protect mRNA-encoding genome editors from degradation; achieve cell-targeted delivery; minimize off-target editing; and overcome physiological barriers, including mucus, macrophages, and endothelial tissues (*11*). More than a billion doses of lipid nanoparticle (LNP)–mRNA COVID-19 vaccines have been administered intramuscularly worldwide, demonstrating high safety and efficacy sustained through repeatable dosing (*12*, *13*). Treatment of genetic lung diseases, including cystic fibrosis (CF), would benefit from direct intravenous (IV) LNP delivery to bypass formidable local intratracheal (*14*) and inhalation (*15*) barriers that include thick, sticky mucus (*16*) and poor access to stem cells at the base of the epithelium. Yet, LNPs predominantly accumulate in the liver when administered intravenously, which hampers extrahepatic therapeutic utility (*17*). In this work, we investigated whether lung selective organ targeting (lung SORT) LNPs (*18*) could access tissue-resident stem cells. We discovered that optimized lung-targeting LNPs can deliver CRISPR-Cas9 endonucleases (*19*) and adenine base editors (ABEs) (*20*) to facilitate the reconstitution of lung epithelium with corrected genes, thereby achieving enduring therapeutic effects.

In this study, we present evidence demonstrating successful lung SORT LNP delivery of Cre recombinase (*Cre*) mRNA, *Cas9* mRNA–single-guide RNA (sgRNA), and *ABE* mRNA-sgRNA to all major lung cell types, including lung stem cells. Notably, we quantified long-term persistence of edited cells for 22 months, highlighting the durable nature of the edits, which has not been achieved in previous studies. Mechanistically, we determined that lung cell types expressing the vitronectin receptor (VtnR), $\alpha_v\beta_3$ integrin, exhibit enhanced editing efficiency. To further illustrate the benefits of editing stem cells, we used CF as a compelling and representative congenital disease model. SORT LNP–mediated base editing effectively corrected the R553X nonsense mutation in mouse lung stem cells and restored cystic fibrosis transmembrane conductance regulator (CFTR) expression and function in organoids derived from mouse intestinal stem cells and in primary human bronchial epithelia derived from people with CF. These findings of effective genome editing in lung stem cells support high feasibility for the creation of long-lasting therapies in genetic lung diseases.

Lung SORT LNPs mediate stem cell delivery to achieve durable editing for >1.8 years

To investigate the potential of lung SORT LNPs to deliver mRNA-encoded gene editors to lung stem cells (*18*, *21*–*23*), we used Ai14 LoxP-stop-LoxP tdTomato (tdTom) reporter mice (*24*), in which removal of the stop cassette orchestrated by Cre recombinase or CRISPR-Cas9 activates tdTom expression, allowing identification of gene-edited cells (Fig. 1A). Mice were administered *Cre* mRNA lung SORT LNPs (LNP-Cre) intravenously (2 mg/kg, two doses 48 hours apart) to evaluate the rates and long-term persistence of genetic changes in the lung after Cre editing. Lung tissues were collected at 10 intervals after the second injection, from 2 to 660 days (Fig. 1B) for ex vivo imaging and flow cytometry. tdTom expression was uniformly spread throughout the mouse lung at every time point (Fig. 1C). tdTom quantification by average radiance (Fig. 1D) and total flux (Fig. 1E) indicated persistence of the tdTom for the entire 660-day experiment.

Basal cells are considered the tissue-specific stem cells in both mouse and human airway

Fig. 1. Direct in vivo gene editing was achieved in mouse lungs and persisted for >1.8 years. (**A**) Schematic representation of LNP-mediated gene editor delivery into lung cells after systemic administration. (**B**) Diagram showing the experimental procedure used to evaluate the efficiency of lung cell editing in Ai14 tdTom reporter mice, in which Cre recombinase can excise the loxP flanked stop cassette, thereby enabling fluorescent tdTom protein expression. Mice were injected with LNP-Cre at 2 mg/kg total RNA (20:1, total lipid to RNA weight ratio) with two sequential doses, 48 hours apart. Mice treated with phosphate-buffered saline (PBS) were used as negative control. (**C**) Ex vivo fluorescence imaging analyses of mouse lungs 2, 7, 21, 42, 60, 120, 180, 360, and 660 days after the last injection. (**D** and **E**) Quantitative analysis of ex vivo lung images was shown as average radiance (D) and as total flux (E). (**F** to **K**) Time-course flow cytometry analyses showing the percentage of tdTom-positive ($tdTOM^+$) cells reported among lung cells (F), endothelial cells (G), immune cells (H), epithelial cells (I), $NGFR^+$ stem cells (J), and $KRT5^+$ stem cells (K). Data are means ± SEMs ($n = 3$ biologically independent replicates) for treated groups.

[1]Department of Biomedical Engineering, Department of Biochemistry, Simmons Comprehensive Cancer Center, Program in Genetic Drug Engineering, The University of Texas Southwestern Medical Center, Dallas, TX 75390, USA. [2]Department of Genetics and Genome Sciences, Case Western Reserve University School of Medicine, Cleveland, OH 44106, USA. [3]ReCode Therapeutics, Menlo Park, CA 94025, USA. [4]Department of Internal Medicine, The University of Texas Southwestern Medical Center, Dallas, TX 75390, USA.
*Corresponding author. Email: daniel.siegwart@utsouthwestern.edu
†These authors contributed equally to this work.

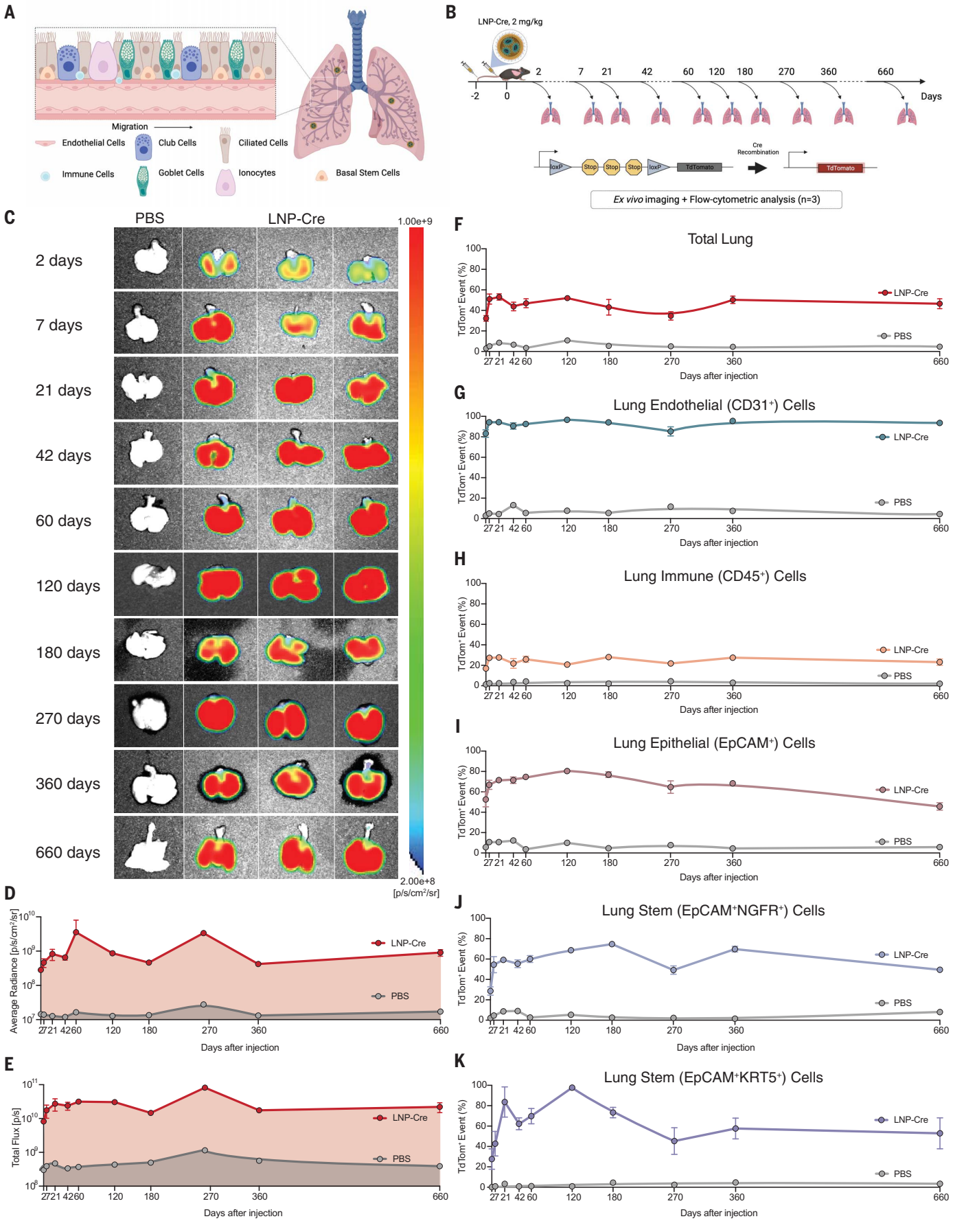

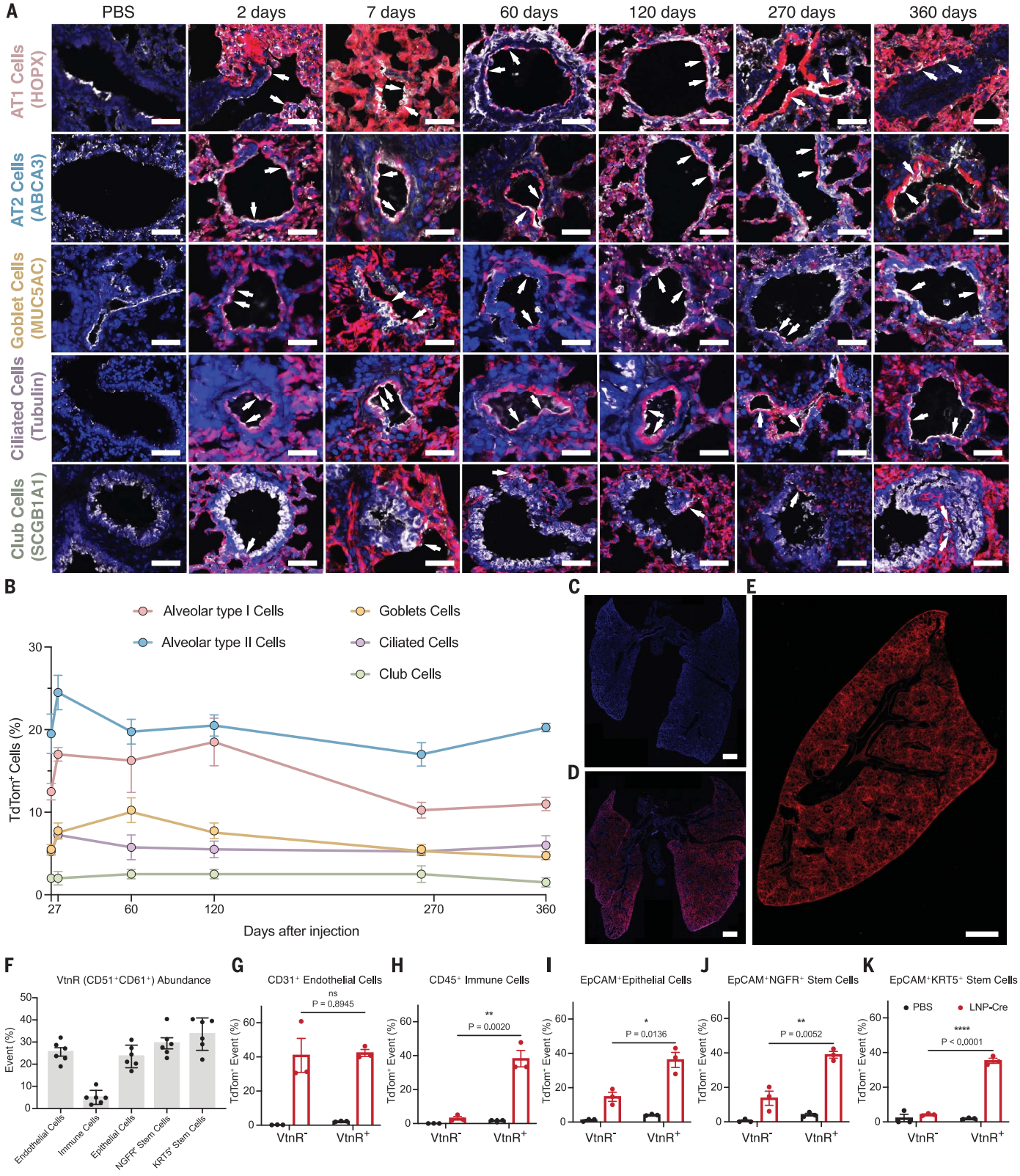

Fig. 2. Lung SORT LNPs mediated efficient delivery into diverse lung cell types with enhanced delivery to VtnR-expressing cells. (**A**) Representative immunofluorescence images of lung sections from LNP-Cre–treated Ai14 reporter mice (2, 7, 60, 120, 270, and 360 days after treatment) to assess LNP-mediated editing in mature lung epithelial cells (HOPX for AT1 cells, ABCA3 for AT2 cells, MUC5AC for goblet cells, tubulin for ciliated cells, and SCGB1A1 for club cells). PBS-treated mice served as negative controls. Scale bars, 30 μm. Markers are white, tdTom are red, and nuclei are blue. (**B**) Quantification of LNP-Cre–mediated editing in mature lung epithelium based on immunofluorescence images. Results were obtained from five to six random segments per whole slide. Data are presented as means ± SEMs. (**C** and **D**) Representative whole-slide immunofluorescence images from

PBS-treated (C) and LNP-Cre–treated (D) mice. 4′,6-diamidino-2-phenylindole (DAPI) is blue, and tdTom is red. Scale bars, 1 mm. (**E**) Representative tissuecyte image of a LNP-Cre–treated mouse's lung whole left lobe (3D rendering provided in movie S1). Scale bar, 1 mm. (**F** to **K**) VtnR ($CD51^+CD61^+$) abundance (F) and quantification of tdTom positivity in $VtnR^+$ ($CD51^+CD61^+$) fraction and $VtnR^-$ ($CD51^-CD61^-$) fraction in lung endothelial cells (G), immune cells (H), epithelial cells (I), $NGFR^+$ cells (J), and $KRT5^+$ stem cells (K). Data are means ± SEMs ($n = 3$ biologically independent replicates). Unpaired *t* test. *P* values of <0.05 were considered statistically significant. ns, not significant.

epithelium, given their capacity to self-renew and their differentiation into various mature cell lineages, including ciliated, secretory, goblet, and ionocytes (*25*–*28*). They can be identified by the expression of nerve growth factor receptor (NGFR) (*28*) or cytoskeletal protein keratin 5 (KRT5) (*29*), both of which were used to ensure a thorough and comprehensive investigation of editing efficiencies. Lineage tracing and clonal growth studies have supported their roles in differentiation and regeneration (supplementary text) (*26*, *28*–*30*).

Flow cytometry analysis revealed that mice had durable editing in a diverse array of lung cell types encompassing endothelial cells ($CD31^+$), epithelial cells ($EpCAM^+$), immune cells ($CD45^+$), and stem cells ($NGFR^+$ and $KRT5^+$) (figs. S1 and S2). More than 32% of all lung cells manifested tdTom-positive ($tdTom^+$) expression 48 hours after the second LNP dose (baseline mark), which subsequently escalated to 51% on day 7 and was sustained throughout the 660-day experiment (Fig. 1F). The editing level was consistently high at the 660-day end point (>93% in endothelial, >23% in immune, and >48% in epithelial) (Fig. 1, G to I). Among $EpCAM^+NGFR^+$ stem cells, 28% showed tdTom expression on day 2, climbing to 75% on day 180, and remaining at 49 to 70% for 660 days (Fig. 1J). Within $EpCAM^+KRT5^+$ stem cells, 27% displayed tdTom expression at 48 hours, peaking to 97% on day 120 and then remaining between 45 and 80% for up to 660 days (Fig. 1K). This dynamic tdTom expression within stem cells may be indicative of mouse stem cell turnover rate over different time intervals (*26*, *28*–*31*).

The general applicability of lung SORT LNPs was further examined with CRISPR-Cas9 as a second editing approach. Lung SORT LNPs encapsulating *Cas9* mRNA and sgTOM1 (*32*) (2:1, wt:wt) (table S1) (LNP-Cas9) were administered intravenously to Ai14 reporter mice (2 mg/kg per dose, three doses 7 days apart). LNP-Cas9 editing yielded persistent tdTom expression across the lungs through the 8-month end point, including in stem cells (fig. S3). Confirming editing in stem cells was encouraging because multiple stop deletions are required to activate tdTOM in this model, which may underestimate CRISPR-Cas9 editing outcomes (*32*). Regarding tolerability, LNP-Cas9 did not alter kidney and liver function up to 240 days at the tested dose and did not cause tissue damage based on hematoxylin and eosin (H&E) staining of mouse hearts and spleens (2 mg/kg total RNA three times) (fig. S4). Lung SORT LNPs facilitated delivery to the trachea, which is involved in the pathophysiology of lung diseases, albeit at a lower overall rate (12.3%) compared with the bronchus (46.9%) (fig. S5). Editing was also observed in CF-affected organs, including the liver, pancreas, kidney, and gastrointestinal tract (fig. S6). A more in-depth characterization revealed 13.5 to 41.7% editing in various lung immune cell types, including neutrophiles (*33*) and macrophages (*34*) (fig. S7). Moreover, delivery efficacy was unchanged in a bacterial infection model with inflamed lungs (fig. S8) (*35*), which suggests that infections common in people with CF may not reduce gene editing.

Long-term editing of diverse cell types in the lungs

The life spans of both lung endothelial cells and lung-resident immune cells range from a few days to several weeks (*36*, *37*). This high turnover rate raises the question of how the editing efficiencies in these cell types were sustained for more than 1.8 years. We hypothesized that lung SORT LNPs edit lung-resident endothelial and immune progenitor cells, ultimately leading to a pool of edited mature cells. Leveraging the endothelial progenitor marker CD157 (BST1) (*38*), we tracked tdTom expression in lung progenitor cells. More than 87% of $CD31^+CD157^+$ cells expressed tdTom at 48 hours, which rose to 95% by day 7 and was sustained for 660 days (fig. S9). Studies also indicate the existence of a pool of lung-resident hematopoietic stem or progenitor cells marked by $Lin^-Sca1^+c\text{-}kit^+$ (LSK) for hematopoietic stem cells (HSCs) and $Lin^-Sca1^-c\text{-}kit^+$ for multipotent progenitors (MPs) (*39*). After IV administration of LNP-Cre, 74% of lung-resident HSCs and 42% of lung-resident MPs expressed tdTom at 48 hours that persisted more than 660 days (fig. S10).

The lung's epithelial lining is made up of assorted cell types performing distinct roles in preserving lung functionality and homeostasis (*40*, *41*). Key epithelial cell types include alveolar type 1 (AT1) for gas-exchange, alveolar type 2 (AT2) for maintaining alveolar homeostasis, goblet cells for mucus production, ciliated cells for mucus removal, club cells for bronchiolar epithelium protection, and rare ionocytes that highly express CFTR (*42*). To delve deeper, we harvested lung tissues at various time points for tissue section imaging (fig. S11 and table S2). Nearly all cell types displayed colocalization of tdTom and their respective cell marker, indicating widespread editing (Fig. 2A). Approximately 18% of AT1 cells, 20% of AT2 cells, 10% of goblet cells, 6% of ciliated cells, and 2% of club cells showed evidence of editing, which persisted for up to 360 days (Fig. 2B). A total of 21.4% of ionocytes were edited by day 2, increasing to 58% at the 660-day mark (fig. S12), which is important because ionocytes control airway surface liquid absorption (*43*, *44*). Whole-section images (Fig. 2, C to E) and three-dimensional (3D) rendering of the entire lung after LNP-Cre treatment revealed a uniform distribution of tdTom expression throughout the lung lobe (movie S1) (*45*, *46*). A second reporter mouse, double-fluorescent mTmG (*47*), was used to further visualize and quantify edited cells (~8% by tissue volume) 2 days after a single LNP-Cre administration that mediated excision to turn on enhanced green fluorescent protein (eGFP) expression replacing preexisting tdTom fluorescent proteins (fig. S13 and movies S2 and S3), further supporting lung SORT LNP–enabled genome editing.

Delivery is enhanced in VtnR-expressing cells

We previously demonstrated that SORT LNPs avidly bind distinct plasma proteins after IV administration, thereby facilitating endogenous targeting of organs and cell types (*48*). We verified that the protein corona of lung SORT LNPs is most highly enriched in vitronectin (fig. S14), which aids uptake in VtnR-expressing cells (*48*). Corroborating with that study, preincubating lung SORT LNPs with vitronectin improved transfection of $VtnR^+$ human bronchial epithelial (16HBE14o-) cells (*49*), but not $VtnR^-$ cells (fig. S15). To further study this mechanism, we analyzed VtnR expression in vivo. Most lung cell types exhibit high levels of VtnR (25.5% of endothelial, 23.5% of epithelial, 29.5% of $EpCAM^+NGFR^+$, and 33.6% of $EpCAM^+KRT5^+$ cells) (Fig. 2F and fig. S16). To evaluate the correlation between VtnR expression and lung SORT LNP–mediated editing, we compared tdTom activation in VtnR-positive ($VtnR^+$, $CD51^+CD61^+$) lung cells versus their VtnR-negative ($VtnR^-$, $CD51^-CD61^-$) counterparts 24 hours after a single LNP-Cre treatment. Lung SORT LNP delivery was greater in $VtnR^+$ epithelial, immune, $EpCAM^+NGFR^+$ stem, and $EpCAM^+KRT5^+$ stem cells compared with $VtnR^-$ fractions (Fig. 2, G to K), indicative of preferential uptake. Endothelial cell delivery was high in $VtnR^+$ and $VtnR^-$ cells at the tested dose (fig. S17). The lung is overall the most VtnR-enriched organ (24.4%) compared with all other organs with <4% VtnR positivity,

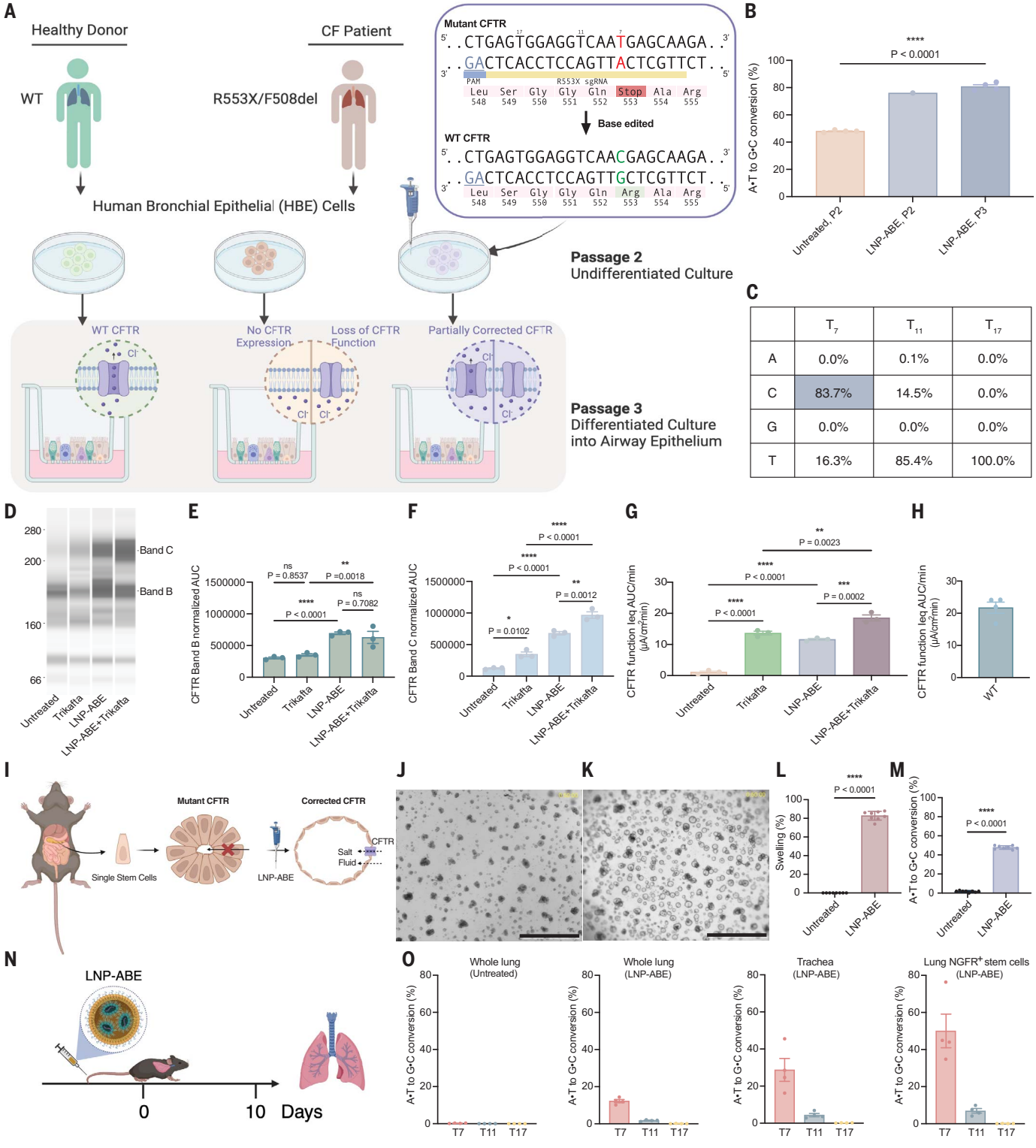

	T_7	T_{11}	T_{17}
A	0.0%	0.1%	0.0%
C	83.7%	14.5%	0.0%
G	0.0%	0.0%	0.0%
T	16.3%	85.4%	100.0%

Fig. 3. Efficient adenine base editing was achieved in lung basal cells in patient-derived HBE cells and CF mouse model. (**A**) Workflow for differentiation of HBEs from a healthy donor and a CF person with CFTR$^{R553X/F508del}$ into airway epithelium and base editing strategy to correct CF R553X mutation. Untreated CF HBE cells were used as negative control, and HBEs from a healthy donor with wild-type (WT) CFTR gene were used for comparison. (**B**) LNP-ABE–mediated 60% of allelic base editing in both undifferentiated P2 (n = 1) and fully differentiated P3 culture (n = 4). (**C**) The frequency of desired product (the box highlighted in blue) and bystander editing was evaluated using NGS sequencing. (**D**) Efficacy of LNP-ABE with or without Trikafta in CFTR protein restoration in CFTR$^{R553X/F508del}$ HBE culture measured by capillary Western blotting. (**E** and **F**) Band B (E) and band C (F) intensities from (D) were normalized to vinculin (20 μg/mL) as an internal standard. Data are means ± SEMs of n = 3 independent replicates. One-way analysis of variance (ANOVA); P values of <0.05 were considered statistically significant. (**G**) Quantitative data for average current calculated from AUC representing CFTR activity further confirmed CFTR restoration.

Data are means ± SEMs of $n = 4$. One-way ANOVA; P values of <0.05 were considered statistically significant. (**H**) CFTR function in HBE culture from non-CF individuals who are wild-type for the *CFTR* gene ($n = 4$ independent replicates). (**I**) Workflow of R553X correction in intestinal organoids using LNP-ABEs and the mechanism of FIS assay. Intestinal stem cells were isolated from R553X homozygous mice to generate intestinal organoids as an ex vivo model to evaluate CFTR function restoration after LNP-ABE treatment. Forskolin-induced CFTR activation can facilitate ion-water transportation leading to organoid swelling. (**J** to **L**) No swelling was observed from untreated group (J), whereas the LNP-ABE–treated group (K) exhibited 80% of intestinal organoid swelling. Scale bars, 1000 μm. (**M**) Approximately 50% base editing was confirmed using DNA sequencing. Data are presented as means ± SEMs of $n = 8$ independent replicates in (L) and (M). Unpaired t test; P values of <0.05 were considered statistically significant. (**N**) Workflow for assessing LNP-ABE–mediated base editing in mouse lung basal cells after a single administration. CF heterozygous R553X mice were injected intravenously with LNP-ABE (1.5 mg/kg total RNA, *ABE* mRNA:sgR553X = 2:1, weight ratio). Mice were euthanized 10 days after the injection. Whole lung tissue, trachea, and isolated lung $NGFR^+$ basal stem cells populations were used for DNA extraction, PCR amplification, and NGS sequencing. (**O**) Base editing efficiency of all adenines within the target protospacer in three lung populations ($n = 4$ independent replicates). Data are presented as means ± SEMs.

which suggests a role for tissue specificity, especially in nonendothelial cell populations (fig. S18). These results emphasize the role of VtnR-mediated uptake of plasma vitronectin-bound lung SORT LNPs.

Efficient editing of primary human CF patient-derived basal cells

To assess the therapeutic potential of lung SORT LNP for genetic lung diseases, we used CF as a representative model, which is caused by mutations in CFTR. Among editing strategies, base editing does not rely on double-stranded break repair, resulting in minimal undesired editing events, even in nondividing cells (*20*, *50*). A base editing strategy (NG-ABE8e), A•T to G•C conversion of the currently untreatable CF nonsense mutation $CFTR^{R553X}$ to wild-type CFTR, has been reported in cells (*51*–*53*). We applied this therapeutic strategy by coencapsulating *ABE* mRNA and sgR553X (table S1) to correct R553X mutation in primary and immortalized human bronchial epithelial (HBE) cells. In engineered 16HBEge CFTR-R553X cells (*49*, *52*), LNP-ABE (*ABE* mRNA:sgRNA = 2:1, wt/wt) treatment led to 95.0% correction by DNA sequencing at 1.5 μg per well dose (fig. S19).

Next, we corrected the R553X mutation in primary CF patient-derived HBE cells (*54*) carrying R553X–F508del compound heterozygous mutations. The difficult-to-treat HBE model differentiates into a pseudostratified epithelium at the air-liquid interface (ALI) that mimics characteristics of in vivo airway biology, allowing strong prediction of therapeutic efficacy in humans (*55*–*57*) (Fig. 3A). After LNP-ABE (1.4 μg total RNA, *ABE* mRNA:sgRNA = 2:1, wt/wt) treatment, ~60% allelic correction was achieved in both undifferentiated P2 culture composed mainly of basal cells and fully differentiated P3 culture analyzed by EditR (*58*) (Fig. 3B). Using next-generation sequencing (NGS) and CRISPResso2 (*59*) analysis, we confirmed a mean 83.7% frequency of the desired product (C nucleotide at T_7), with moderate bystander editing (14.5%) at T_{11} and no editing at T_{17} (Fig. 3C). Bystander editing at the T_{11} position should be neutral in effect because both GGT and GGC encode glycine (*52*).

To evaluate the CFTR protein expression restoration after LNP-ABE treatment, we performed capillary Western blotting (Fig. 3D and fig. S20). LNP-ABE alone doubled the expression of core glycosylated CFTR (Fig. 3, D and E, band B) and increased the expression of fully glycosylated, mature CFTR by 5.5-fold (Fig. 3, D and F, band C). Combined treatment with LNP-ABE and the CFTR modulator Trikafta [elexacaftor/tezacaftor/ivacaftor, standard-of-care for CF people with F508del mutations (*60*)] further increased the expression of fully glycosylated CFTR by 7.8-fold (Fig. 3, D and F, band C).

We tested the ability of LNP-ABE to restore HBE function by measuring CFTR-dependent Cl^- channel activity 4 weeks after the LNP-ABE treatment using transepithelial current clamp (TECC) assay. LNP-ABE alone effectively restored 53.4% of the CFTR function [area under the curve (AUC) = 11.6 $\mu A/cm^2$ min] (Fig. 3G) compared with the activity of wild-type CFTR measured from HBE culture derived from an individual without CF, presumed to have 100% CFTR activity (AUC = 21.7 $\mu A/cm^2$ min) (Fig. 3H), which greatly exceeds the widely accepted therapeutic threshold for CFTR activity restoration of >10% to prevent CF disease symptoms (*61*). CFTR function was further boosted to 85% restoration by the combination of LNP-ABE and Trikafta (AUC = 18.5 $\mu A/cm^2$ min) (Fig. 3G). Considering the nature of heterozygous CF HBE models, we acknowledge that higher CFTR function might be achieved with LNP-ABE in homozygous models. We also assessed lung SORT LNP delivery of tdTomato mRNA (LNP-tdTom) in differentiated HBEs from the basolateral side to mimic in vivo systemic delivery to the lungs, which confirmed >50% transfection of basal cells (fig. S21). Together, our results suggest that efficient correction of undifferentiated lung basal cells can successfully produce corrected mature epithelium and restore CFTR function.

In vivo stem cell editing in CF mouse lungs

We next evaluated LNP-ABE–mediated editing in genetically engineered CF mice harboring the whole human exon 12 containing R553X replacing the endogenous mouse exon (materials and methods) to study R553X correction in the local human sequence context. Despite having the R553X nonsense mutation, the model does not exhibit pathological features in the lung, consistent with other CF mouse models (*62*). To address this constraint, we isolated intestinal stem cells from homozygous R553X mice and generated intestinal organoids [forskolin-induced swelling (FIS) assay] (*62*, *63*) to assess restoration of CFTR function (Fig. 3, I to K, and movies S4 and S5). More than 82% of organoids swelled after LNP-ABE treatment (Fig. 3L). In total, 47.8% of A•T to G•C conversion was confirmed by DNA sequencing (Fig. 3M). These findings demonstrate the capacity to remedy pathological features of CF in cells derived from R553X mice.

To assess the feasibility of base editing in lung stem cells for potential long-lasting effect, we used heterozygous R553X mice with one allele carrying the locally humanized R553X mutation and one normal mouse CFTR allele. By using a specifically designed pair of primers, only the human R553X region was amplified by polymerase chain reaction (PCR) for sequencing analysis (table S3). LNP-ABE was administered intravenously at 1.5 mg/kg total RNA (ABE mRNA:HM sgR553X = 2:1, weight ratio) (table S4) (*64*, *65*). Ten days after a single treatment, mouse lungs were collected. Genomic DNA was extracted from whole lungs, trachea, and lung stem cells isolated from whole-lung single-cell suspension using magnetic-based cell separation (Fig. 3N) for PCR amplification and NGS sequencing. In total, 50.0% correction at the desired T_7 position in lung stem cells, 12.2% in the whole lung, and 28.7% in the trachea were quantified (Fig. 3O). These results suggest that LNP-ABE can efficiently correct the target pathogenic mutation in mouse lung stem cells.

Discussion

It is increasingly apparent that genome editing in lung stem cells could provide a lasting therapy for genetic lung diseases. Acknowledging historical and recent advances in viral vectors for gene therapy (*66*–*69*) and lung delivery (*70*, *71*), packaging limits, immunogenicity, and the risk of gene disruption have hindered

success in genome editing. Compared with viral and other nonviral aerosolized delivery approaches, IV-administered SORT LNPs may have greater access to lung basal stem cells given the lack of disease-related mucosal barriers and the immediate proximity of the lung endothelial bed to LNPs (*72*). In this work, we demonstrated that lung SORT LNPs deliver mRNA, CRISPR-Cas9, and base editor components to various lung cells, including stem cells. Tracking of edited cells for 22 months revealed that the degree of editing was consistently maintained across the lungs during this entire period, suggesting further differentiation to mature cells.

Endogenous targeting is a plausible mechanism to aid lung accumulation and cellular uptake. We acknowledge that other factors, such as transcytosis (*73*), recycling endosomes (*74*), passage through tight junctions (*75*), and exosome-macrophage transfer (*76*), could contribute to the delivery process (*17*). Although VtnR expression may explain enrichment of SORT LNPs in lung cells, there may be vitronectin-dependent and -independent processes involved in endothelial cell delivery. Given that SORT LNPs access deeper tissue structures through the vasculature, reduced expression of VtnR in nonlung organs (*77*) could be one factor that contributes to the selectivity of SORT LNPs. Additional protein corona–related factors could contribute to the observed lung tissue enrichment by reduced binding of proteins associated with liver uptake (*78*) and increased binding of proteins involved in avoiding clearance mechanisms (*48*, *79*). Future studies exploring these areas will be instrumental in increasing our understanding of these complex mechanisms.

Lung SORT LNPs facilitated delivery of base editors to achieve gene correction in nearly 50% of lung stem cells in a CF mouse model carrying the R553X mutation, paving the way for therapeutic intervention in CF and other diseases. SORT LNPs effectively delivered base editors to correct the *CFTR* and restore function in primary R553X–F508del HBEs. These transwell functional readouts predict clinical benefit, having supported the approval of clinically used CFTR modulators (*55*–*57*).

Future research is required to deepen our mechanistic understanding of lung SORT LNP delivery to stem cells, assess therapeutic effectiveness of LNP-ABE in phenotypic CF animal models, and evaluate cellular targeting and safety in nonhuman primates. Ultimately, our findings of durable correction of pathogenic mutations in tissue-resident stem cells highlight the potential of producing long-term cures through the targeted delivery of gene editing systems for a variety of diseases.

REFERENCES AND NOTES

1. J. Y. Wang, J. A. Doudna, *Science* **379**, eadd8643 (2023).
2. C. A. Hodges, R. A. Conlon, *Genes Dis.* **6**, 97–108 (2018).
3. K. A. Hajj, K. A. Whitehead, *Nat. Rev. Mater.* **2**, 17056 (2017).
4. T. Wei *et al*., *ACS Nano* **14**, 9243–9262 (2020).
5. A. Raguram, S. Banskota, D. R. Liu, *Cell* **185**, 2806–2827 (2022).
6. J. D. Gillmore *et al*., *N. Engl. J. Med.* **385**, 493–502 (2021).
7. J. G. Rurik *et al*., *Science* **375**, 91–96 (2022).
8. L. Xu *et al*., *Mol. Ther.* **25**, 1782–1789 (2017).
9. N. E. King *et al*., *Hum. Gene Ther.* **31**, 956–972 (2020).
10. S. Suzuki *et al*., *Mol. Ther.* **28**, 1684–1695 (2020).
11. A. McCarron, P. Cmielewski, V. Drysdale, D. Parsons, M. Donnelley, *Gene Ther.* **30**, 469–477 (2023).
12. F. P. Polack *et al*., *N. Engl. J. Med.* **383**, 2603–2615 (2020).
13. L. R. Baden *et al*., *N. Engl. J. Med.* **384**, 403–416 (2021).
14. B. Li *et al*., *Nat. Biotechnol.* **41**, 1410–1415 (2023).
15. A. K. Patel *et al*., *Adv. Mater.* **31**, e1805116 (2019).
16. F. Ratjen *et al*., *Nat. Rev. Dis. Primers* **1**, 15010 (2015).
17. S. A. Dilliard, D. J. Siegwart, *Nat. Rev. Mater.* **8**, 282–300 (2023).
18. Q. Cheng *et al*., *Nat. Nanotechnol.* **15**, 313–320 (2020).
19. M. Jinek *et al*., *Science* **337**, 816–821 (2012).
20. N. M. Gaudelli *et al*., *Nature* **551**, 464–471 (2017).
21. K. Zhou *et al*., *Proc. Natl. Acad. Sci. U.S.A.* **113**, 520–525 (2016).
22. X. Wang *et al*., *Nat. Protoc.* **18**, 265–291 (2023).
23. T. Wei, Q. Cheng, Y.-L. Min, E. N. Olson, D. J. Siegwart, *Nat. Commun.* **11**, 3232 (2020).
24. L. Madisen *et al*., *Nat. Neurosci.* **13**, 133–140 (2010).
25. D. T. Montoro *et al*., *Nature* **560**, 319–324 (2018).
26. J. R. Rock, S. H. Randell, B. L. Hogan, *Dis. Model. Mech.* **3**, 545–556 (2010).
27. Y. Zhou *et al*., *eLife* **11**, e80083 (2022).
28. J. R. Rock *et al*., *Proc. Natl. Acad. Sci. U.S.A.* **106**, 12771–12775 (2009).
29. W. Zuo *et al*., *Nature* **517**, 616–620 (2015).
30. P. A. Kumar *et al*., *Cell* **147**, 525–538 (2011).
31. A. E. Vaughan *et al*., *Nature* **517**, 621–625 (2015).
32. B. T. Staahl *et al*., *Nat. Biotechnol.* **35**, 431–434 (2017).
33. L. M. Yonker *et al*., *J. Cyst. Fibros.* **20**, 1062–1071 (2021).
34. J. L. Gillan *et al*., *Sci. Adv.* **9**, eadg5128 (2023).
35. S. Abid *et al*., *Infect. Immun.* **85**, 10.1128/iai.00422-17 (2017).
36. D. H. Bowden, *Am. Rev. Respir. Dis.* **128**, S46–S48 (1983).
37. I. Y. R. Adamson, in *Toxicology of Inhaled Materials: General Principles of Inhalation Toxicology*, H. P. Witschi, J. D. Brain, Eds. (Springer, 1985), pp. 289–317.
38. T. Wakabayashi *et al*., *Cell Stem Cell* **22**, 384–397.e6 (2018).
39. E. Lefrançais *et al*., *Nature* **544**, 105–109 (2017).
40. D. N. Kotton, E. E. Morrisey, *Nat. Med.* **20**, 822–832 (2014).
41. B. L. M. Hogan *et al*., *Cell Stem Cell* **15**, 123–138 (2014).
42. L. W. Plasschaert *et al*., *Nature* **560**, 377–381 (2018).
43. F. Yuan *et al*., *Nature* **621**, 857–867 (2023).
44. L. Lei *et al*., *J. Clin. Invest.* **133**, e171268 (2023).
45. T. Klouda *et al*., *Front. Med.* **7**, 343 (2020).
46. D. M. O. Ramirez, A. D. Ajay, M. P. Goldberg, J. P. Meeks, in *Multiphoton Microscopy*, E. Hartveit, Ed. (Springer, 2019), pp. 195–224.
47. M. D. Muzumdar, B. Tasic, K. Miyamichi, L. Li, L. Luo, *Genesis* **45**, 593–605 (2007).
48. S. A. Dilliard, Q. Cheng, D. J. Siegwart, *Proc. Natl. Acad. Sci. U.S.A.* **118**, e2109256118 (2021).
49. H. C. Valley *et al*., *J. Cyst. Fibros.* **18**, 476–483 (2019).
50. G. A. Newby, D. R. Liu, *Mol. Ther.* **29**, 3107–3124 (2021).
51. M. H. Geurts *et al*., *Cell Stem Cell* **26**, 503–510.e7 (2020).
52. S. Krishnamurthy *et al*., *Nucleic Acids Res.* **49**, 10558–10572 (2021).
53. M. F. Richter *et al*., *Nat. Biotechnol.* **38**, 883–891 (2020).
54. D. M. Cholon, M. Gentzsch, *Curr. Opin. Pharmacol.* **64**, 102210 (2022).
55. J. P. Clancy *et al*., *J. Cyst. Fibros.* **18**, 22–34 (2019).
56. F. Van Goor *et al*., *Proc. Natl. Acad. Sci. U.S.A.* **106**, 18825–18830 (2009).
57. F. Van Goor *et al*., *Proc. Natl. Acad. Sci. U.S.A.* **108**, 18843–18848 (2011).
58. M. G. Kluesner *et al*., *CRISPR J.* **1**, 239–250 (2018).
59. K. Clement *et al*., *Nat. Biotechnol.* **37**, 224–226 (2019).
60. P. G. Middleton *et al*., *N. Engl. J. Med.* **381**, 1809–1819 (2019).
61. S. M. Rowe, F. Accurso, J. P. Clancy, *Proc. Am. Thorac. Soc.* **4**, 387–398 (2007).
62. D. R. McHugh *et al*., *PLOS ONE* **13**, e0199573 (2018).
63. J. F. Dekkers *et al*., *Nat. Med.* **19**, 939–945 (2013).
64. D. E. Ryan *et al*., *Biochemistry* **62**, 3512–3520 (2023).
65. H. Yin *et al*., *Nat. Biotechnol.* **35**, 1179–1187 (2017).
66. A. L. Cooney, P. B. McCray Jr., P. L. Sinn, *Genes* **9**, 538 (2018).
67. E. W. F. W. Alton *et al*., *Thorax* **72**, 137–147 (2017).
68. D. Vidović *et al*., *Am. J. Respir. Crit. Care Med.* **193**, 288–298 (2016).
69. L. S. Ostedgaard *et al*., *Proc. Natl. Acad. Sci. U.S.A.* **99**, 3093–3098 (2002).
70. Z. Yan *et al*., *Hum. Gene Ther.* **33**, 1023–1036 (2022).
71. M. K. Yanda *et al*., *Hum. Gene Ther.* **34**, 1135–1144 (2023).
72. N. Bertrand, J.-C. Leroux, *J. Control. Release* **161**, 152–163 (2012).
73. G. W. Liu, E. B. Guzman, N. Menon, R. S. Langer, *Pharm. Res.* **40**, 3–25 (2023).
74. P. Paramasivam *et al*., *J. Cell Biol.* **221**, e202110137 (2022).
75. Y. Zhang, W.-X. Yang, *Beilstein J. Nanotechnol.* **7**, 675–684 (2016).
76. M. Maugeri *et al*., *Nat. Commun.* **10**, 4333 (2019).
77. B. Singh, C. Fu, J. Bhattacharya, *Am. J. Physiol. Lung Cell. Mol. Physiol.* **278**, L217–L226 (2000).
78. A. Akinc *et al*., *Mol. Ther.* **18**, 1357–1364 (2010).
79. S. A. Dilliard *et al*., *J. Control. Release* **361**, 361–372 (2023).

ACKNOWLEDGMENTS

We appreciate and thank the people with CF who donated their primary airway cells. We thank H. Valley and the Cystic Fibrosis Foundation (CFF) Therapeutics Lab for providing cells and advice; A. Nawaby, D. Ramirez, and A. Farwell from the University of Texas Southwestern (UTSW) Whole Brain Microscopy Facility (RR:SCR_017949) for helping with lung 3D imaging and rendering; J. Gong, J. Mao, and K. Dague for help with preparing formulations; Z. Wang for help with HBE staining protocol; J. M. Shelton from UTSW Histo Pathology Core for helping with histology; M. Xu and C. Lewis from the UTSW Tissue Management Share Resource for helping with immunostaining and slide scanning; the UTSW Small Animal Imaging Shared Resource; the UTSW McDermott Center Sanger Sequencing Core; and A. Lemoff from the UTSW Proteomics Core, the UTSW Metabolic Phenotyping Core, the Moody Foundation Flow Cytometry Facility, and the CF Mouse Model Resource Center at Case Western Reserve University (CWRU). **Funding:** This work was supported primarily by CFF (SIEGWA18XX0, SIEGWA21XX0, HODGES19R1, and CONLON18G0) and in part by the National Institutes of Health (NIH) National Institute of Biomedical Imaging and Bioengineering (NIBIB) (R01 EB025192-01A1) and a Sponsored Research Agreement with ReCode Therapeutics. The UTSW Small Animal Imaging Shared Resource is supported in part by the NCI (P30CA142543) and CPRIT (RP210099). **Author contributions:** Conceptualization: Y.S., S.C., and D.J.S. Methodology: Y.S. and S.C. Investigation: Y.S., S.C., X.L., Z.T., S.R.S., Y.X., S.A.D., Y.-C.S., M.K., S.M.L., S.M., X.W., D.Z., S.W., P.B., J.W., J.L., R.J.M., D.F.L., W.J., S.A., M.H., A.M., B.A.W., D.J.L., R.J., R.A.C., and M.L.D. Visualization: Y.S., S.C., and D.J.S. Resources: C.A.H. and D.J.S. Project administration: S.C. and D.J.S. Supervision: C.A.H., S.C., and D.J.S. Writing – original draft: Y.S., S.C., and D.J.S. Writing – review & editing: C.A.H. and D.J.S. Funding acquisition: R.A.C., M.L.D., C.A.H., and D.J.S. **Competing interests:** A provisional patent application covering compositions, methods, and uses for targeting CF and related disorders has been filed by UTSW naming Y.S. and D.J.S. as inventors. D.J.S. is a cofounder and member of the scientific advisory board of ReCode Therapeutics, which has licensed intellectual property from UTSW. D.J.S. discloses financial interests in ReCode Therapeutics, Signify Bio, and Tome Biosciences. R.J. serves on the Recode clinical advisory committee. S.R.S., J.W., J.L., M.H., A.M., and B.A.W. are employees of ReCode Therapeutics. D.J.L. is the President and CSO of ReCode Therapeutics and has stock options in the company. All other authors declare that they have no competing interests. **Data and materials availability:** All data are available in the main text or the supplementary materials. All data needed to evaluate the conclusions in the paper are present in the main text or supplementary materials. DNA sequencing files can be accessed at the National Center for Biotechnology Information Sequence Read Archive (NCBI SRA) with accession code PRJNA1064574.

SUPPLEMENTARY MATERIALS

science.org/doi/10.1126/science.adk9428
Materials and Methods
Supplementary Text
Figs. S1 to S21
Tables S1 to S4
MDAR Reproducibility Checklist
Movies S1 to S5

Submitted 20 September 2023; accepted 17 April 2024
10.1126/science.adk9428

Science
AAAS

Supplementary Materials for

In vivo editing of lung stem cells for durable gene correction in mice

Yehui Sun *et al*.

Corresponding author: Daniel J. Siegwart, daniel.siegwart@utsouthwestern.edu

Science **384**, 1196 (2024)
DOI: 10.1126/science.adk9428

The PDF file includes:

Materials and Methods
Supplementary Text
Figs. S1 to S21
Tables S1 to S4

Other Supplementary Material for this manuscript includes the following:

MDAR Reproducibility Checklist
Movies S1 to S5

Materials and Methods

Lipid nanoparticle formulation

5A2-SC8 was synthesized and purified by following published protocols (*21*, *22*). 1,2-dioleoyl-sn-glycero-3-phosphoethanolamine (DOPE, Cat# 850725) and 1,2-dioleoyl-3-trimethylammonium-propane (DOTAP, Cat# 890890) were purchased from Avanti Polar Lipids. Cholesterol (Cat# C3045) was purchased from Sigma-30 Aldrich. 1,2-Dimyristoyl-rac-glycero-3-methylpolyoxyethylene (DMG-PEG2000, Cat# GM-020) was purchased from NOF America Corporation. D-Lin-MC3-DMA (Cat# 555308) was purchased from MedKoo Biosciences. LNPs were prepared by following published protocol (*22*). In brief, an aqueous phase with RNA cargos was rapidly mixed with an organic phase congaing the lipids at a 3:1 volume ratio. The organic phase was prepared by dissolving 5A2-SC8, DOPE, cholesterol, DMG-PEG and DOTAP in ethanol at given molar ratio (32.4:18:36:3.6:10 for in vitro studies; 21.6:12:24:2.4:40 for in vivo studies). The aqueous phase contains RNA cargos in citrate buffer (pH 4). The total lipid to RNA weight ratio was 20:1. LNPs were formed by either vortex mixing or T-mixing, then dialyzed (Pur-A-Lyzer Midi Dialysis Kits, WMCO 3.5 kDa, Cat# PURX35100) against 1 x phosphate buffered saline (PBS) for 3 hours before usage. The particle size, polydispersity index, and zeta potential of LNPs were measured using dynamic light scattering (DLS) (Zetasizer Nano ZS machine, Malvern, v.7.13) and the RNA encapsulation efficiency were measured using Quant-iT RiboGreen RNA assay (Invitrogen, Cat# R11491) following published protocols (*22*).

In vitro transcribed mRNA and chemically modified sgRNA

mRNAs encoding Cre recombinase, Cas9, NG-ABE8e were synthesized by in vitro transcription (IVT). NG-ABE8e was a gift from Professor David Liu (Addgene plasmid # 138491 ; http://n2t.net/addgene:138491 ; RRID:Addgene_138491) (*53*). The coding fragments of each protein were cloned into a pCS2+MT plasmid backbone featuring a SP6 promoter, customized 5' and 3' untranslated regions (UTR) as well as a poly(A) segment through NEBuilder HiFi DNA assembly (NEB, Cat# E2621S). IVT was conducted using the MEGAscript SP6 transcription kit (Invitrogen, Cat# AM1330) with N1-methylpseudouridine-5'-triphosphate replacing the typical uridine triphosphate. Next, a Cap1 cap structure was installed to the 5' end of the mRNA using the Cap1 Capping System (Hongene, Cat# ON-028 & ON-014). Luciferase mRNA and tdTomato mRNA was provided by ReCode Therapeutics. All mRNAs were purified using LiCl and the integrity of the purified mRNAs was monitored by High Sensitivity RNA ScreenTape System (Agilent, Cat# 5067-5579).

sgRNAs (sgTOM1 and sgR553X) were purchased from and synthesized by Agilent using solid phase synthesis and phosphoramidite chemistry. All sgRNAs were incorporated with end modification (3 x 2′-O-methyl-3′-phosphorothioate (MS) on 5' end and 3 x 2′-O-methyl-3′-phosphonoacetat (MP) on 3' end (*64*)). Heavily modified sgR553X (HM sgR553X) was utilized for *in vivo* base editing experiment by following a previously reported modification pattern (*65*). The sequences of sgRNA used are shown in **Table S1**.

Animal experiments

Animal experiments were approved by the Institution Animal Care and Use Committee of The University of Texas Southwestern Medical Center under animal protocols (#2016-101430 and # 2016-101897) or the Institutional Animal Care and Use Committee of Case Western Reserve University under animal protocols (#2014-0064)), and were consistent with local, state, and federal

regulations as applicable. Ai14 mice (Strain #:007914, RRID:IMSR_JAX:007914) and mT/mG mice (Strain #:007676, RRID:IMSR_JAX:007676) were purchased from The Jackson Laboratory and bred to maintain the homozygous strains at the UTSW Animal Facility. All animals were maintained on a 12/12-h light/dark schedule at a mean temperature of 22 °C. Heterozygous and homozygous R553X CF mice created at Case Western Reserve University were used for in vivo base editing studies at CWRU. All experiments were performed with sample sizes calculated by power analyses.

Cell lines and primary cells

The immortalized, CFTR wild-type expressing human bronchial epithelial cells, 16HBE14o- (generated by D. Gruenert) was gene edited at the endogenous CFTR locus using CRISPR-Cas9 to create isogenic 16HBEge CFTR R553X and 16HBEge CFTR F508del (M470) cell lines (*49*). The 16HBEge CFTR R553X and 16HBEge CFTR F508del (M470) cells were provided by the Cystic Fibrosis Foundation Therapeutics Lab.

Primary HBE cells were collected from transplanted lungs from a healthy donor (DD0059J) who has wild-type $CFTR^{wt/wt}$ and an individual with cystic fibrosis (20180717CF) who was heterozygous for $CFTR^{R553X/F508del}$. Primary HBE cells were provided by the Cystic Fibrosis Foundation Therapeutic Lab.

In vivo long-term lung cell editing study

For gene editing in mice lungs with LNP-Cre, 8-week-old Ai14 mice were randomly allocated to either LNP-Cre-treated group or PBS-treated group. The mice were injected with 200 μL of LNP-Cre formulation at 2 mg/kg (*Cre* mRNA) twice, 2 days apart. Animals were euthanized at different time points over a total of 660 days (2 days, 7 days, 21 days, 42 days, 60 days, 120 days, 180 days, 270 days,360, and 660 days after the last injection). To study in vivo lung cell editing, lungs were either collected for ex vivo fluorescence imaging (AMI-HTX, Spectral Instruments Imaging) followed by FACS analysis or fixed with 4% PFA for two days followed by 10%-18% sucrose for frozen sectioning with the assistance of the UTSW Histo Pathology Core and immunofluorescence staining with HOPX, MUC5AC, Tubulin, SCGB1A1 and ABCA3 antibodies (**Table S2**) with assistance provided by the UTSW Tissue Management Core.

To investigate the potential of Lung SORT LNPs to deliver CRISPR-Cas9/sgRNA system in Ai14 mice, a previously developed sgRNA (sg298 or sgTOM1, **Table S1**) was utilized (*32*). Unlike Cre recombinase, which is highly efficient in LoxP deletion, tdTom activation induced by the CRISPR-Cas9 system necessitates double or triple deletion of the STOP cassettes which underestimates the efficacy of LNP-Cas9-mediated editing. For gene editing in mice lungs with LNP-Cas9, 8-week-old Ai14 mice were randomly allocated to either LNP-Cas9-treated group or PBS-treated group. The mice were injected with 200 μL of LNP-Cre formulation at 2 mg/kg total RNA (*Cas9* mRNA:sgTOM1=2:1, wt/wt) three times, one week apart. Animals were euthanized at different time points over a total of 240 days (7 days, 21 days, 60 days, 120 days, 120 days, 240 days after the last injection) (**Fig. S3**). Lung tissues were collected for FACS analysis to study in vivo lung cell editing, heart and spleen tissues were collected for histopathology evaluation (sections and H&E staining were prepared by UT Southwestern Tissue Management Shared Resource, the slides were scanned using Vectra Polaris from Akoya Biosciences at 20X magnification and digitalized using Phenochart software), and serum separated from whole blood were collected to measure liver function (AST and ALT) and kidney function (BUN and CREA) (analysis performed by the UT Southwestern Metabolic Phenotyping Core)

LNP treatment in mice with acute infection and inflammation in lungs

The acute infection mouse model was generated by following a published protocol (*35*). 8-week-old Ai14 mice were randomly allocated to P. aeruginosa infection group or non-infection group. P. aeruginosa strain PAO1 was obtained from ATCC . Bacteria colonies were streaked onto Trypticase soy agar (TSA) plates from frozen glycerol stocks and incubated overnight at 37°C. Overnight cultures were washed in 150 nM sodium chloride, and the resulting pellets were resuspended in 1 ml of Luria-Bertani (LB) broth. Culture concentrations were determined based on the optical density at 600 nm (OD600) and the previously determined number of CFU for each strain, to give the CFU/OD600. Mice in the infection group were inoculated intranasally with 50 ul of P.aeruginosa at 3.5 x 10^5 CFU to generate acute infection model. The previous study found neutrophil number and cytokine expression evaluated 9 h after P. aeruginosa infection in mouse lungs (*35*). To investigate the delivery efficiency of LNP in infected and inflamed lungs, mice were injected with either LNP-Cre formulation at 2 mg/kg (*Cre* mRNA) or PBS 9 hr post P. aeruginosa infection. Animals were euthanized 24 hr after LNP-Cre treatment, followed by FACS analysis of lung cells to study editing efficiency.

Isolation of single cells from mouse tissues

Mouse lungs, tracheas and other organs were extracted and immediately placed in ice-cold PBS. These tissues were then cut into small pieces and moved into a 50 mL tube containing 10 mL of 1X lung tissue digestion media [RPMI digestion medium (1:1 vol/vol): RPMI supplemented with 2% wt/vol BSA, 300 U/mL collagenase, and 100 U/mL hyaluronidase]. The 50 mL tube was placed in an incubator set at 37 °C for an hour, with continuous shaking at a speed of 180 rpm. After incubation, the homogenized lung cell solution was agitated using a pipette to disperse any clumps of cells, then it was filtered into a new 50 mL Falcon tube through a 100-micron strainer. The strainer was rinsed using 10 mL of a wash buffer composed of chilled PBS and 2% Fetal Bovine Serum (FBS). Afterwards, the sample was centrifuged at a speed of 1200 rpm for 5 minutes. Following this step, the supernatant was removed, and the remaining cell pellet was reconstituted in 10 mL of the chilled wash buffer. Subsequently, the sample was spun at 1200 rpm for 5 minutes. Next, the cell pellet was treated with 5 mL of 1X RBC lysis buffer (BioLegend, Cat# 420301) at room temperature for 5 minutes to eliminate any red blood cells. After the lysis procedure, 10 mL of wash media was added to the sample, which was subsequently spun at 1200 rpm for another 5 minutes. The final cell pellet, which was now free from red blood cells, was reconstituted in 5 mL of cell staining buffer (BioLegend, Cat# 420201). Finally, the sample was subjected to antibody staining in preparation for flow cytometry.

To examine whether Lung SORT LNPs facilitate mRNA delivery to the tracheal region of the lung and enable cell editing, LNP-Cre were intravenously administered to Ai14 mice in two successive doses, each being 2 mg/kg 48 hours apart. Tracheas (**Fig. S5A**) were extracted 48 hours following the final injection, and tdTom expression across various cell types was quantified using flow cytometry. The composition of cells markedly differed between the trachea and bronchus regions of the lung. The trachea harbored more immune cells (~55.8%) and fewer epithelial (~13.7%) and endothelial cells (~8.4%) compared to the bronchus (35.4% immune cells, 28.7% epithelial cells, and 23.5% endothelial cells) (**Fig. S5A**). Overall, the percentage of total edited cells was lower in the trachea (~12%) compared to the bronchus (~46%) (**Fig. S5B**). Among the various cell types, barring edited endothelial cells which were 70.7% in the trachea and 88.3% bronchus (high in both trachea and bronchus), the percentage of edited immune cells (5.6% in

trachea vs. 37.8% in bronchus), epithelial cells (16.4% in trachea vs. 71.7% in bronchus), basal epithelial cells (12.0% in trachea vs. 59.9% in bronchus), and epithelial stem cells (12.2% in trachea vs. 67.9% in bronchus) was lower in the trachea compared to the bronchus region (**Fig. S5B-G**). This difference could be attributed to the challenges faced by the lung SORT LNPs in navigating and reaching the tracheal part of the lung. Regardless, Lung SORT LNPs also reach the trachea following IV administration and achieve genome editing.

Antibody staining of single cells from mouse tissues and analysis by flow cytometry

Single-cell suspensions, derived from the mouse lungs and other organs, were initially blocked with mouse Fc-receptor blocker (Thermo Fisher, Cat# 14-9161-73) for a period of 15 minutes. After that, the cells were marked with a variety of antibodies, namely Alexa Fluor 488-conjugated anti-mouse CD31 (BioLegend, Cat# 102414), Pacific Blue-conjugated anti-mouse CD45 (BioLegend, Cat# 103126), Alexa Fluor 647-conjugated anti-mouse EpCAM (BioLegend, Cat# 118212), APC-conjugated anti-mouse CD157 (BioLegend, Cat# 140207), PerCP Cy5-5-conjugated anti-mouse Sca1 (Invitrogen, Cat# 45-5981-80), Alexa Fluor 700-conjugated anti-mouse CD117 (Thermo Fisher, Cat# 56-1172-80), FITC-conjugated anti-mouse lineage cocktail antibodies (BioLegend, Cat# 133302), unconjugated anti-mouse NGFR (LS Bio, Cat# LS-C179536), PE/Cyanine7-conjugated anti-mouse/rat CD61 (BioLegend, Cat# 104317),Brilliant Violet 711-conjugated anti-mouse CD51 (Fisher Scientific, Cat# BDB740755), FITC-conjugated anti-mouse CD3 (BioLegend, Cat# 100203), FITC-conjugated anti-mouse Ly-6G (BioLegend, Cat# 108405), FITC-conjugated anti-mouse CD11b (BioLegend, Cat# 101205), FITC-conjugated anti-mouse TER-119 (BioLegend, Cat# 116205), APC-conjugated anti-mouse B220 (BioLegend, Cat# 103211), Alexa Fluor 700-conjugated anti-mouse CD8 (Thermo Fisher, Cat# 56-0081-80), PerCP-conjugated anti-mouse CD4 (BioLegend, Cat# 100431), APC-conjugated anti-mouse Ly-6G (BioLegend, Cat# 127613), Alexa Fluor 594-conjugated anti-mouse F4/80 (BioLegend, Cat# 123140), PerCP/Cy5.5-conjugated anti-mouse CD11c (BioLegend, Cat# 117327). This labeling process involved incubating a 100 µL portion of the cell suspension with 1 µL these antibodies for 15 minutes, while keeping on ice. Dead cells within the suspension were identified using Ghost Dye Red (Tonbo Bioscience, Cat# 13-0865-T100). Following this, the cell pellet was washed thrice with cell staining buffer to eliminate excess antibodies. The NGFR-stained cells were further stained with a rat secondary Alexa Fluor 488-conjugated antibody (Thermo Fisher, Cat# A48262) for 15 minutes on ice. Finally, the cell pellet was resuspended in 500 µL of cold cell staining buffer and kept on ice until it was ready for analysis through a flow cytometer. The cells were subsequently analyzed using a Becton Dickenson (BD) LSR Fortessa flow cytometer. Finally, the data collected from the flow cytometer were processed and analyzed using Flowjo software (BD).

For intracellular flow cytometry, the EpCAM-stained cell pellet was resuspended in 500 µL of fix/perm solution, part of the BD Fix/Perm kit (BD Bioscience, Cat# 554714) and left on ice for 20 minutes. Following this, the cells were centrifuged at 1200 rpm for 5 minutes to obtain cell pellet. The pellet was then washed three times with 1X fix/perm wash buffer (the kit supplied a 10X concentration, which was diluted to 1X with MilliQ water), before being prepared for antibody staining. Subsequently, 100 µL of the fixed and permeabilized EpCAM-stained cells were incubated with 1 µL of an unconjugated anti-mouse KRT5 antibody (Abcam, Cat# ab52635) for a duration of 30 minutes. After this incubation period, the cells were washed three times with 1X fix/perm wash buffer to remove any surplus antibody, and then resuspended in 100 µL of 1X fix/perm buffer. In the subsequent step, 100 µL of the KRT5-labelled cells were incubated with 1 µL of an Alexa Fluor 488-conjugated anti-rabbit secondary antibody on ice for an additional 30

minutes. Finally, after another three washes with 1X fix/perm wash buffer, the cell pellet was resuspended in 500 µL of cold 1X fix/perm wash buffer and kept on ice until it was ready for analysis through a flow cytometer.

For intracellular FOXI1 staining, the cell pellet was resuspended in 500 µL of fix/perm solution, part of the BD Fix/Perm kit (BD Bioscience, Cat# 554714) and left on ice for 20 minutes. Following this, the cells were centrifuged at 1200 rpm for 5 minutes to obtain cell pellet. The pellet was then washed three times with 1X fix/perm wash buffer (the kit supplied a 10X concentration, which was diluted to 1X with MilliQ water), before being prepared for antibody staining. Subsequently, 100 µL of the fixed and permeabilized cells were incubated with 1 µL of an Alexa Fluor 647 conjugated anti-mouse FOXI1 antibody (Novus Biologicals, Cat# NBP2-70747AF647) for a duration of 30 minutes. After this incubation period, the cells were washed three times with 1X fix/perm wash buffer to remove any surplus antibody. Finally, the cell pellet was resuspended in 500 µL of cold 1X fix/perm wash buffer and kept on ice until it was ready for analysis by a flow cytometer.

Magnetic cell separation of cells isolated from mouse lungs

To isolate NGFR positive cells from the snap freezed lungs, we employed the mouse biotin positive selection kit (Stem Cell Technologies, Cat# 17665) and adhered to the manufacturer's instructions. In brief, we incubated 5 $x10^6$ RBC-depleted cells in 100 µL of cell staining buffer (BioLegend, Cat# 420201) with 1 µL of FcR blocker (Thermo Fisher, Cat# 14-9161-73) and 1 µL of biotin-conjugated anti-mouse NGFR antibody (Thermo Fisher, Cat# P75NTR-BIOTIN) at room temperature for 15 minutes. Next, we added 10 µL of biotin selection cocktail to the cell suspension and incubated for another 15 minutes at room temperature. Finally, 5 µL of streptavidin-bound magnetic nanoparticles was added to the cell suspension and incubated for 10 minutes at room temperature. The cell suspension was then adjusted to a total volume of 2.5 mL by adding 2.4 mL of cell staining buffer in a 5 mL falcon tube and was subjected to a magnet for 5 minutes. The magnet was then placed at a 45-degree angle, enabling us to decant off the supernatant. The NGFR positive cell fraction, which had adhered to the tube, was dislodged from the magnet by washing the tubes with 500 µL of fresh cell staining buffer. Lastly, the magnetic nanoparticles bound cells were centrifuged at 1200 rpm for 5 minutes to obtain the final cell pellet.

Immunofluorescence

For Immunofluorescence studies, mouse lung samples were fixed with 4% paraformaldehyde for two days at 4 °C then equilibrated in 10% sucrose for 12 hr followed by 18% sucrose for another 12 hr before proceeding with cryosectioning with assistance from the UTSW Histo Pathology Core. Slides were then stained with HOPX, MUC5AC, Tubulin, SCGB1A1, and ABCA3 antibodies (**Table S2**) of lung cells and later imaged with assistance from the UTSW Tissue Management Core. The frozen tissues mounted on charged glass slides were dried for 30 minutes at 37 °C on a slide warmer (Slide Moat from Boekel Scientific, model 240000) followed by 15 minutes at room temperature. The slides were rehydrated in a wash buffer (Leica, Cat# AR9590) for 10 minutes and then loaded into the Leica Bond RX. The slides were incubated with unconjugated primary antibody for 20 minutes followed by goat anti-mouse secondary antibody with Alexa Fluor 647 (Biolegend, Cat# 405322, 1:200) or donkey anti-rabbit secondary antibody with Alexa Fluor 647 (Biolegend, Cat# 406414, 1:200) for 30 minutes. All slides were mounted with ProLong Gold Antifade Mountant with DNA Stain DAPI (Invitrogen, Cat# P36931). The slides were scanned using Vectra Polaris from Akoya Biosciences at 20X magnification and

digitalized using Phenochart software. Five to six random segments from each whole slide immunofluorence images for each mouse lung were used to generate quantification analysis. Editing efficiency was calculated as tdTomato^{+}Alexa Fluor 647^{+} cells/Fluor 647^{+} cells and expressed as a percentage.

TissueCyte 3D imaging and analysis

Inflated lung tissues were prepared by following a published protocol (*45*) and used for vibratome sectioning and tissuecyte 3D imaging. In brief, mouse trachea was cannulated with 22 g blunt-ended needle and inflated with 2.5–4 mL 2% agarose solution. The dissected lungs were incubated in 4% paraformaldehyde solution overnight at 4 °C. The next day, the left lobe of the lungs was washed with 1 X PBS at 4 °C and stored for future use.

A modified agarose embedding method was employed for the lungs used in this study, which incorporated infiltration of the inflated lung with acrylamide prior to agarose embedding. The lungs were soaked overnight at 4 °C in a solution of Surecast (ThermoFisher, Cat# HC2040), with a total concentration of 4% Surecast and 0.5% VA-044 activator, in excess volume (5 mL per lung lobe), diluted in phosphate buffer (PB; 0.42 g/L monobasic sodium phosphate, 0.92 g/L dibasic sodium phosphate). The lungs were then allowed to equilibrate to room temperature for 1 hour while gently shaking. Each lung was transferred to a cryomold (VWR, Cat# 15160-215), which was filled with the prepared acrylamide solution. The mold was covered securely with foil and incubated in an oven at 40 °C for two hours. After polymerization was complete, the excess acrylamide was carefully removed from around the lung. The acrylamide-infused tissue was then embedded in oxidized agarose for vibratome sectioning and TissueCyte imaging as previously described (*46*).

Images of serial tissue sections were collected throughout the volume of the lung using the Tissuecyte 1000 Two-Photon Tomography system with integrated vibratome. Samples were imaged using a two photon laser with 920 nm excitation wavelength and 3-channel PMT detectors (Red >560 nm, Green 500-560 nm, Blue <500 nm) as contiguous overlapping tiles on each serial section. Serial blockface sections were cut with the integrated vibratome (60 hz) spaced 75 μm apart and each serial section was imaged at three Z-focal plane levels spaced 25 μm apart. Contiguous overlapping image tiles for each section and focal plane were stitched using the UT Autostitch software (Tissuevision). Overlapping tile regions were aligned based on xy coordinates and specified overlap parameter (95%) and alpha blended to form the whole section image. Average tile intensity values from the first 60 slices were used to perform brightness adjustment on all tiles prior to stitching to improve section uniformity. Stitched whole section images from the three focal planes collected for each section were downsampled to 1.5 microns per pixel, merged as a maximum intensity projection (MIP), and color adjusted for visual contrast fidelity by eye using a Matlab script. For the Ai14 mouse lung rendering, whole lung volumes of the red channel of the contrast adjusted MIP tissue images were resampled to 800 z slices using bilinear interpolation to improve rendering smoothness, and visualized in Fiji's 3D viewer. For the mTmG mouse lung rendering, once the merging and color adjustment were complete, a subsample of MIP color adjusted section images from the whole lung volume were selected for the training portion of the machine learning based signal segmentation pipeline. Machine learning training for GFP signal segmentation was done in the Ilastik software, using the default parallel random forest implementation. Selected features used as discriminators in the model were Gaussian Smoothing (sigma = 0.3-5.0), Laplacian of Gaussian (sigma = 0.3-5.0), Gaussian Gradient Magnitude (sigma = 0.3-5.0), Difference of Gaussians (sigma = 0.3-5.0), Structure Tensor Eigenvalues (sigma = 0.3-

5.0), Hessian of Gaussian Eigenvalues (sigma = 0.3-5.0). In Ilastik, an annotator labeled pixels from selected section images as either GFP signal or background classes (background, tissue autofluorescence, and bubbles). These annotations were used to train the classifier. Once the annotator labeled enough pixels to be satisfied with the classification accuracy, predictions for GFP signal on all of the lung volume sections were exported as 8 bit probability maps: per pixel intensity mappings separated by class, in which higher intensity values represent a higher classifier certainty that the classification of that pixel is correct.

The exported probability maps were used to perform quantification on the classified GFP signal. Using a thresholded version of the MIP images, a selection mask of the tissue area in the images was created. This mask was applied to the GFP probability map to select predicted GFP signal that was within the tissue boundaries. Then the summed intensity values and summed intensity values per unit volume (mm^3) were calculated using a Matlab script. The percent area calculation was done by determining a threshold level (threshold = 101) for the probability map by eye to determine the classifier certainty level where visible GFP signal looked correctly segmented, and then applying the same determined threshold to both samples. Then the total volume of positive thresholded GFP signal within the tissue area was quantified and divided by the total tissue volume using an ImageJ script to obtain the final percent area measurement.

Whole lung volumes were resampled to 800 – z slices using bilinear interpolation to improve rendering smoothness, and visualized in Fiji's 3D viewer.

Mass spectrometry proteomics analysis of plasma proteins absorbed on Lung SORT LNPs

The previously described approach was used to isolate plasma proteins that interact with the Lung SORTLNPs used in this study (*48*). In brief, C57BL6/J mouse plasma (Fisher Scientific, Cat# NC0961764) was added to LNP-Cre solution (1 g/L, total lipid content), at a 1:1 volume ratio and incubated for 15 min at 37 °C. The LNP/plasma mixture was loaded onto a 0.7 M sucrose in MilliQ water cushion of equal volume to the mixture and centrifuged for 1 hour at 15,300 g and 4 °C. The supernatant was removed, and the pellet was washed with 1× PBS. The pellet was centrifuged at 15,300 g and 4 °C for another 5 min to remove washing buffer. Washing was repeated twice more for a total of three washes. After the final wash, the pellet was resuspended in 2 wt. % SDS. Excess lipids were removed using ReadyPrep 2-D Cleanup (Bio-Rad, Cat# 1632130) following the manufacturer recommended protocol. The resulting pellet was resuspended in 2× Laemmli buffer.

To prepare the sample for mass spectrometry proteomics, 10 μL of the plasma protein mixture isolated from the LNPs was loaded on to a 4-20% TGX gel. The sample was run at 90 V for 10 min, to enable stacking. To fix and visualize the proteins, the gel was stained with Bio-Safe Coomassie. After 1 hour of destaining, the protein band was cut out using a razor blade and diced into a small cube with a volume of nearly 1 mm^3. The cubes were then placed in a 1.5 mL Eppendorf tube and kept at 4 °C until they were analyzed by mass spectrometry at the UTSW Proteomics Core. The protein contents were identified and quantified using a Thermo QExactive HF mass spectrometer. The identified proteins were sorted according to their abundance/MW. A custom Python Script was created to rank the most abundant proteins and plot them as a heat map and classify the physiological classes of the identified proteins.

Code used for protein corona composition analysis

```
import pandas as pd
import numpy as np
```

```
import requests as r
import matplotlib.pyplot as plt
import seaborn as sns
from Bio import SeqIO
from Bio.SeqUtils.ProtParam import ProteinAnalysis
from io import StringIO
def load_protein_corona(corona_file):
    corona = pd.read_excel(corona_file, index_col = 'Accession')
    corona = corona.fillna(0)
    return corona

def collate_corona_files(corona_list, to_copy, sample_names):
    corona_data_subset = []
    for i in range(len(corona_list)):
        corona_data_subset.append(corona_list[i][['Description', to_copy]])
        corona_data_subset[i].columns = ['Description', sample_names[i]]
    all_coronas = pd.concat(corona_data_subset, axis=1, copy=False)
    all_coronas['Description'] = all_coronas['Description'].fillna('')
    grouped_coronas = pd.DataFrame()
    grouped_coronas['Description'] =
all_coronas['Description'].groupby(level=0,axis=1).max()
    for sample_name in sample_names:
        grouped_coronas = grouped_coronas.join(all_coronas[sample_name])
    grouped_coronas = grouped_coronas.fillna(0)
    return grouped_coronas

def filter_proteins(corona_df, threshold):
    clean_corona_df = corona_df.copy()
    for i in range(len(corona_df)):
        single_protein = corona_df.iloc[i,1:]
        row_name = single_protein.name
        if single_protein.max() < threshold:
            clean_corona_df = clean_corona_df.drop(row_name)
    return clean_corona_df

def proteins_heatmap(corona_df, show_variant=False):
    sample_start = corona_df.columns.get_loc('Description') + 1
    corona_abundances = corona_df.iloc[:,sample_start:]
    new_names = []
    if show_variant:
        protein_names = corona_df.Description.tolist()
        for protein in protein_names:
            split_name = protein.split(' OS')
            var_num_location = split_name[1].find('SV')
            var_num = split_name[1][var_num_location:]
            new_names.append(split_name[0] + ' ' + var_num)
```

```
        corona_abundances.index = new_names
    else:
        protein_names = corona_df.Description.tolist()
        for protein in protein_names:
            split_name = protein.split(' OS')
            new_names.append(split_name[0])
        corona_abundances.index = new_names
    color_choice = sns.cubehelix_palette(as_cmap=True)
    plt.figure(figsize=(50,25))
    sns.heatmap(corona_abundances, cmap=color_choice, yticklabels=1)
    plt.xticks(rotation=0)
    sns.set(font_scale=2)

def cluster_proteins(corona_df, show_variant=False):
    sample_start = corona_df.columns.get_loc('Description') + 1
    corona_abundances = corona_df.iloc[:,sample_start:]
        new_names = []
    if show_variant:
        protein_names = corona_df.Description.tolist()
        for protein in protein_names:
            split_name = protein.split(' OS')
            var_num_location = split_name[1].find('SV')
            var_num = split_name[1][var_num_location:]
            new_names.append(split_name[0] + ' ' + var_num)
        corona_abundances.index = new_names
    else:
        protein_names = corona_df.Description.tolist()
        for protein in protein_names:
            split_name = protein.split(' OS')
            new_names.append(split_name[0])
        corona_abundances.index = new_names
    color_choice = sns.cubehelix_palette(as_cmap=True)
    sns.clustermap(corona_abundances, cmap=color_choice, yticklabels=1, figsize = (50,40))

def average_proteins(corona_df, replicates, sample_names):
    replicate_average = []
    column_names = [sample_names[i][:-2] for i in range(0,len(sample_names),replicates)]
    average_corona_df = pd.DataFrame(index = corona_df.index)
    average_corona_df['Description'] = corona_df['Description']
    for i in range(1, len(sample_names),replicates):
        replicate_df = corona_df.iloc[:,i:i+replicates]
        replicate_average = replicate_df.mean(axis=1).tolist()
        sample_index = int((i-1)/replicates)
        average_corona_df[column_names[sample_index]] = replicate_average
    return average_corona_df
```

```
def classify_proteins(corona_df):
    protein_classes = pd.read_excel('Protein Classification.xlsx')
    protein_classes = protein_classes.fillna('')
    classified_proteins = pd.DataFrame(index= corona_df.columns[1:],
    columns= protein_classes.columns)
    classified_proteins = classified_proteins.fillna(0)
    for i in range(1,len(corona_df)-1):
        row = corona_df.iloc[i,:]
        prot_acc = row.name
        for column in protein_classes:
            if prot_acc in protein_classes[column].values:
                classified_proteins[column] += row
    classified_proteins = classified_proteins.transpose()
    return(classified_proteins)

def get_prot_sequences(accession_list):
    proteins = []
    baseUrl="http://www.uniprot.org/uniprot/"
    for accession in accession_list:
        currentUrl=baseUrl+accession+".fasta"
        response = r.post(currentUrl)
        cData=''.join(response.text)
        Seq=StringIO(cData)
        pSeq=list(SeqIO.parse(Seq,'fasta'))
        if len(pSeq) > 0:
            proteins.append(pSeq[0].seq)
    return proteins

def prot_analysis(prot_seqs, prot_names):
    pI_list = [] # isoelectric point
    aromaticity_list = [] # aromaticity
    hydropathy_list = [] # GRAVY score
    helix_list = [] # % protein with helix structure
    turn_list = [] # % protein with turn structure
    sheet_list= [] # % protein with sheet structure
    charge_list = [] # protein charge at pH 7.4
    for seq in prot_seqs:
        seq = str(seq)
        seq = seq.replace("X","G")
        seq = seq.replace("U","G")
        seq = seq.replace("B","G")
        seq = seq.replace("Z","G")
        prot_data = ProteinAnalysis(seq)
        pI_list.append(prot_data.isoelectric_point())
        aromaticity_list.append(prot_data.aromaticity())
        hydropathy_list.append(prot_data.gravy())
```

```
        charge_list.append(prot_data.charge_at_pH(7.4))
        secondary_structure = prot_data.secondary_structure_fraction()
        helix_list.append(secondary_structure[0])
        turn_list.append(secondary_structure[1])
        sheet_list.append(secondary_structure[2])

    protein_properties = pd.DataFrame(index=prot_names)
    protein_properties['pI'] = pI_list
    protein_properties['Aromaticity'] = aromaticity_list
    protein_properties['Hydropathy'] = hydropathy_list
    protein_properties['Charge at pH = 7.4'] = charge_list
    protein_properties['Helix'] = helix_list
    protein_properties['Turn'] = turn_list
    protein_properties['Sheet'] = sheet_list
    return protein_properties

def weighted_avg(property_series, corona_df):
    property_df = pd.DataFrame(index=property_series.index,
    columns= corona_df.columns)
    for column in corona_df.columns:
        perc_abun = corona_df[column].tolist()
        renorm_abun = [i/sum(perc_abun) for i in perc_abun]
        corona_df[column] = renorm_abun
    for protein in corona_df.index:
        property_val = property_series[protein]
        property_df.loc[protein] = corona_df.loc[protein]*property_val
    weighted_property = property_df.sum(axis=0)
    return weighted_property

base_file_name = 'PCF-SD-5502--02--2023_'
min_sample_ID = 1066959
max_sample_ID = 1066994
replicates = 3
corona_list = []
names_df = pd.read_excel('Sample Names.xlsx')
sample_names = names_df['Samples'].tolist()
for i in range(min_sample_ID, max_sample_ID + 1):
    corona_list.append(load_protein_corona(base_file_name + str(i) + '_PD2.xlsx'))
grouped_coronas = collate_corona_files(corona_list, 'Abundance/MW', sample_names)
grouped_coronas = grouped_coronas.sort_values(by = 'Description')
grouped_coronas.to_excel('Grouped Coronas.xlsx')

filtered_coronas = filter_proteins(grouped_coronas.copy(), 6.5*10**5)
filtered_coronas.to_excel('Filtered Coronas.xlsx')
average_corona = average_proteins(filtered_coronas, replicates, sample_names)
average_corona.to_excel('Averaged Coronas.xlsx')
```

```
proteins_heatmap(average_corona) # standard heatmap
#cluster_proteins(filtered_coronas) # hierarchical clustering
classified_df = classify_proteins(average_corona)
classified_df.to_excel('Protein Pie Charts.xlsx')
accession_list = filtered_coronas.index.tolist()
proteins = get_prot_sequences(accession_list)
sequences_df = pd.DataFrame(proteins)
prot_props = prot_analysis(proteins, filtered_coronas.index)
properties_of_interest = ['Charge at pH = 7.4', 'Aromaticity',
                          'Hydropathy', 'Helix', 'Turn', 'Sheet']
avg_property_df = pd.DataFrame(columns=properties_of_interest,
                               index=filtered_coronas.columns[1:])
for property_type in properties_of_interest:
    avg_property = weighted_avg(prot_props[property_type],
                                filtered_coronas[filtered_coronas.columns[1:]])
    avg_property_df[property_type] = avg_property
avg_property_df.to_excel('Protein Properties.xlsx')
print('Done')
```

LNPs treatment in 16HBE14o- with R553X mutations

16HBE14o- human bronchial epithelial cells with R553X mutation were maintained in complete growth media composed of Minimum Essential Medium (Gibco, Cat#11095-072) with 10% Fetal Bovine Serum (Gibco, Cat#26140-079) and 1% Penicillin/Streptomycin (Gibco, Cat#15140-122). Plates and flasks were coated with LHC basal medium (Gibco, Cat#12677-027) with 1.34 µL/mL Bovine serum albumin 7.5% (Gibco, Cat#15260-037), 10 µL/mL Bovine collagen solution, Type 1 (Advanced BioMatrix, Cat#5005-100mL), 10 µL/mL Fibronectin from human plasma (1mg/mL) (Thermofisher, Cat#33016-015) by 2h incubation at 37 °C followed by thorough removal of coating solution and storage at 4 °C up to three months. Cells were thawed into a T75 flask at a seeding density of 1×10^6 per flask in complete growth media and incubated at 37 °C for 3 days until confluency. Medium was changed three times a week. For the LNP-ABEs treatment, cells were seeded onto a 6-well plate with a seeding density of 3×10^5 cells/well in 2 mL of complete growth media. Cells were incubated overnight to reach 80% confluency and the media was replaced with fresh complete growth media before LNP-ABEs treatment. For the treatment, 100 µL of LNP-ABE were added to each well at 80% cell confluency stage and 48 h post-treatment, 1 mL of complete growth media was added to each well. 72 h post-treatment, cells were collected using TrypLE Express (Gibco, Cat# 12604-021).

LNP-ABE treatment in undifferentiated HBE cells with CF R553X/F508del mutation

Cystic fibrosis patient derived HBE cells with compound heterozygous mutation of R553X/F508del (passage 2, P2) were thawed and seeded at 1.3×10^5 cells/well on 6-well plates precoated with 3T3 conditioned media (Cell culture core, Rosalind Franklin University of Medicine and Science), with daily maintenance in BEGM Bronchial Epithelial Cell Growth Medium (Lonza, Cat# CC3170). At day 4, undifferentiated cells were treated with 100 µL of 1.4 µg/well of LNP-ABEs, with media change 48 h post-treatment. An untreated group was used as the negative control. Once confluent at day 6, cells were established on transwell inserts for cell differentiation (passage 3, P3) with seeding at 1.5×10^5 cells/insert (Corning, #3378; HTS

Transwell®-24-well permeable support with 0.4 µm pore polyester membrane and 6.5 mm inserts) with complete growth medium on both apical and basal sides. After 24 hrs, the inserts were changed to a 2% UG Differentiating medium (Cell Culture Core, Rosalind Franklin University of Medicine and Science). After 96 h, cultures were brought to the Air-liquid interface (ALI). Cultures were maintained for 4 weeks with media change every other day. The fully differentiated HBEs were finally detached from the inserts by adding ice-cold Accumax (Cat# 00-4666-56, Thermofisher) and incubating at 37 °C for 30 min for further analyses.

CFTR quantification using Jess™ capillary western blot

P3 R553X/F508del HBE cells were lysed immediately following TECC-24 functional analysis. After removing the media from the basolateral side, cells were washed with 100 µL of 1X DPBS at room temperature. 35 µL of RIPA buffer (Rockland Immunochemical, Cat# MB-077-0050) with 1% HALT (Thermofisher, Cat# 78442), 1% 0.5M EDTA (15575-038), 0.5% Universal Nuclease (Thermofisher, Cat# 88702) was then added directly to the apical side of the insert. After 30 min at 4 °C on a plate shaker, cell lysates were collected, and insoluble fractions were separated by centrifugation at 15,000 rpm for 5 minutes at 4 °C. Supernatant were transferred to new tubes and amount of protein in the cell lysates was measured using a bicinchoninic acid (BCA) assay (Thermofisher, Cat# 23227). The lysates were then diluted to a final concentration of 1.5 µg /µL in a 5x fluorescent master mix (ProteinSimple, EZ standard pack 1), and 3 µL was added per well to the JESS microplate. Polyclonal rabbit IgG anti-human CFTR antibody (Atlas, Cat# HPA021939) was used at 3 µg/mL and the monoclonal mouse IgG2A anti-Vinculin antibody (R&D systems, Cat# MAB6896) was used at 20 µg/mL concentration. For secondary antibodies (ProteinSimple, Anti-Rabbit detection module, Cat# DM-001, and Anti-Mouse detection module, Cat# DM-002), and chemiluminescence were used as per kit instructions. Additional reagents including Ab-diluent, washing buffer, and capillary cartridges were used from the 66-440 kDa Separation Module (SM-W004-1, ProteinSimple, Bio-Techne). The manufacturer's protocol was followed to perform the JESS™ capillary western blot instrument (ProteinSimple, Bio-Techne, Minneapolis, MN, USA). The results were analyzed using Compass for Simple Western software.

Measurement of CFTR function in fully differentiated HBE cells

Post-treatment, undifferentiated HBE R553X/F508del cells at P3 were subjected to differentiation for 4 weeks. Once differentiated, CFTR function in the HBE cells was measured as transepithelial chloride secretion using a Transepithelial Current Clamp (TECC) and a 24-well electrode manifold (EP Devices). 4 days prior to the small molecule treatment, selected wells were washed with 3 mM DTT (Roche Diagnostics, Cat# 10197777001) for 30 mins at 37 °C. 24 h before the small molecule treatment, cells were washed with 1X DPBS (Gibco, Cat# 14190-144,) for 30 mins at 37 °C then incubated for 24 hrs with either Trikafta or control vehicle 0.2% DMSO (Fisher Scientific, Cat# BP231100). To prepare the plate for functional assay, differentiation media was replaced with HEPES buffered F-12 assay medium (pH 7.4) on both apical and basolateral sides. After an incubation of 45 minutes at 37 °C without CO_2, the plate was mounted onto a 37 °C heated platform, and transepithelial resistance (Rt) and voltage (Vt) were continuously measured using the TECC device. Baseline values were first measured for 30 minutes, then Rt and Vt were measured (1) for 15 minutes after apical addition of benzamil (Sigma, Cat# 2417) (6 µM final concentration); (2) for 30 minutes after simultaneous apical/basolateral addition of forskolin (Sigma, Cat# F6886) (10 µM final concentration)/VX-770 (Selleckchem chemicals, Cat# S1144) (1 µM final concentration); (3) and for 15 minutes after basolateral addition of bumetanide (Sigma,

Cat# B3023) (20 µM final concentration). CFTR functional results are presented as equivalent chloride current (Ieq) which was calculated using Ohm's law, Ieq = Vt/Rt.

LNP-tdTom treatment in fully differentiated HBE cells with CF R553X/F508del mutation

Cystic fibrosis patient derived HBE cells with compound heterozygous mutation of R553X/F508del (passage 2, P2) were thawed and seeded in BEGM growth medium on flasks precoated with 3T3 conditioned media. Once confluent at day 5, undifferentiated cells were established on Falcon inserts with complete growth medium on both apical and basal sides. After reaching full confluency on inserts, cultures were then brought to the Air-liquid interface (ALI) in 2% UG Differentiating medium (Cell Culture Core, Rosalind Franklin University of Medicine and Science). Cultures were maintained for 23 days with media change every other day. Cells were then treated with 50 µL of LNP-tdTom (12 ug tdTom mRNA per well, 30:1 total lipid to mRNA weight ratio) either to the apical side in liquid bolus for 8 h or to the basolateral side containing 650 µL of differential media for 24h. An untreated group was used as the negative control. Cells were finally collected using Accumax (Sigma, #SCR006).

Antibody staining and analysis by flow cytometry of the treated differentiated HBE cells

Collected cells were resuspended using the LIVE/DEAD™ Fixable Scarlet (723) Viability Kit (Thermofisher, #L34987) and fixed using 4% PFA for 10 min at RT. Cells were then permeabilized by adding eBioscience™ Permeabilization Buffer (Life Technologies, #00-8333-56) for 10 min at RT. Fc Receptor blocker (Biolegend, Human TrueStain FcX, #422302) was then used to block the cells in staining buffer (permeabilization buffer + 0.5% BSA) for 30 minutes at RT. Cells were first incubated uteroglobin/SCGB1A1 Antibody (Novus Biologicals LLC #MAB4218) for 50 min at RT and goat anti-rat IgG with Alexa Fluor 405 (ABCAM #ab175671) on ice for 30 min . After washing, the cells were marked with a variety of primary antibodies, namely Alexa Fluor 647-conjugated Anti-Cytokeratin 5 antibody (Abcam #ab193895), Alexa Fluor 750-conjugated Acetyl--Tubulin (Lys40) (D20G3) XP Rabbit mAb (Cell Signaling Technology #87488S), Alex Fluor 488 conjugated Mucin 5AC [45M1] mouse mAb (Abcam # ab309610-100UL) for 50 min at RT. After PBS wash and resuspension in PBS 0.5% BSA, samples were subsequently analyzed using a Thermofisher Attune Cytpix flow cytometer. Finally, the data collected from the flow cytometer were processed and analyzed using Flowjo software (BD).

LNPs treatment in A-498, Huh-7 and 16HBE14o- cells

A-498 cells were obtained from ATCC. Huh-7 cells were a kind gift from Dr. Hao Zhu's lab. A-498, Huh-7, or 16HBE14o- with F508del mutation were cultured in white-bottom 96-well plates at a density of 1×10^4 cells per well the day before transfection. The white-bottom 96-well plates for 16HBE14o- were pre-coated by coating solution as previously described and all cells were cultured in the medium as recommended by the suppliers. SORT LNPs (5A2-SC8/DOPE/cholesterol/DMG-PEG/DOTAP=21.6:12:24:2.4:40 molar ratio, total lipids/mRNA = 20/1, wt/wt) and non-SORT LNPs (MC3/DSPC/cholesterol/DMG-PEG=50/10/38.5/1.5 molar ratio, total lipids/mRNA = 20/1, wt/wt) containing luciferase (*Luc*) mRNA were prepared by vertex mixing using published protocol (*22*).

For vitronectin pre-coating assay, SORT and non-SORT LNPs containing *Luc* mRNA were incubated with or without 0.25 g vitronectin/g total lipid of human vitronectin (Thermo Fisher, Cat# A14700) for 15 minutes at 37°C. Then the culture was treated with either native LNPs or vitronectin-coated LNPs (25 ng of *Luc* mRNA per well, n=4). After 24 h, *Luc* mRNA expression

was quantified by ONE-Glo + Tox kits (Promega, Cat# E7120) 24 h after the treatment by following Promega's standard protocol.

For vitronectin competitive assay, cells were incubated with human vitronectin by replacing culture media with the vitronectin-contained medium at 0.2 μg vitronectin/mL concentration prior LNP treatment. After 10-min incubation, vitronectin-coated LNPs (0.25 g vitronectin/g total lipid) were added into each well with 25 ng *Luc* mRNA (n=4). Following 4 h co-incubation, each well was washed with PBS one time and replaced with the fresh medium without vitronectin. After 24 h, *Luc* mRNA expression was quantified by ONE-Glo + Tox kits (Promega, Cat# E7120) 24 h after the treatment by following Promega's standard protocol.

Generation of the partially humanized exon replacement R553X mice

To produce the partially humanized *R553X* mouse *Cftr* allele (*Cftr*^{R553X}) we replaced mouse exon 12 and flanking intronic sequences (130 bp upstream; 89 bp downstream) with the corresponding human sequence exon 12 containing the R553X mutation.

Candidate guide RNAs (gRNA) in the introns surrounding exon 12 of mouse *Cftr* were tested *in vitro* using Guide-It gRNA *in vitro* transcription and screening kit (Takara) and two active guides were chosen (5'-GGCACTTGAGTTTATATGAT-3' for intron 11 and 5'-ATCAATTCCAGAGACAGAAC-3' for intron 12). A targeting vector plasmid was constructed containing the human sequences and 1 kb arms homologous to the mouse genome. The gRNAs (5 ng/μL each; Synthego), targeting vector plasmid (1ng/μL; VectorBuilder) and Cas9 protein (10 ng/μL; PNABio) were injected in the pronucleus of C57BL/6J zygotes. Embryos were transferred to pseudo-pregnant females. Founders were identified by genotyping and sequencing for correct integration of human exon 12 sequence.

Mice homozygous for the R553X mutation were created by breeding heterozygous males and females. Genotyping was completed by PCR analysis using DNA extracts from ear biopsies. Genotyping was completed to distinguish between alleles of mouse exon 12 and human exon 12 (R553X). To detect the human exon 12 containing R553X allele (205 bp) primers P1 (5'-AGAAGGAAGATGTGCCTTTCA -3') and P2 (5'-CAAATGCTTGCTAGACCAATAATTAGT -3') were used. To detect the mouse exon 12 (WT) allele (312 bp) primers P3 (5'- TGGGCTTATGGGTAGTCTTTGA-3') and P4 (5'-CAGGAAGCAGAAGAGAAATGTGT -3') were used in a single reaction. Primers were selected to surrounding introns since human and mouse exon 12 are highly homologous. PCR reactions were completed for 40 cycles of 95 °C for 30 seconds, 55 °C for 30 seconds and 72 °C for 30 seconds and products were run out on 2% agarose gels. All mice were allowed unrestricted access to water and solid chow (Envigo, Teklad S-2335 breeder diet, Cat# 7904). All animals were maintained on a 12-h light, 12-h dark schedule at a mean ambient temperature of 22 °C and were housed in standard polysulfone microisolator cages in ventilated units with corncob bedding.

Crypt harvest and intestinal organoid culture

Intestinal organoids were cultured similar to previously described methods (*62*). Mice were euthanized by CO_2 asphyxiation, and 20 cm of intestine measured from the stomach were removed. Fecal matter was flushed from the intestine with Ca^{2+}- and Mg^{2+}-free PBS, and the intestine was flayed using dissecting scissors. The villi were scraped from the small intestine using a microscope slide, and the intestine was cut into ~1 cm segments, which were suspended in 2 mM EDTA in Ca^{2+}- and Mg^{2+}-free PBS. The intestinal segments were incubated on a shaker for 30 minutes at room temperature. The segments were then vortexed at for 10 seconds, allowed to settle, and then

the supernatant was removed and stored in a 10 cm dish. This process was repeated until four supernatant fractions were produced. The fractions were inspected under a microscope, and the fraction which was most enriched for crypts was passed through a 70 μm cell strainer. The crypts were pelleted at 1,000xG for 10 minutes, then resuspended in 1:1 mixture of Intesticult Organoid Growth Media (STEMCELL Technologies, Cat# # 06005) and MatriGel (Corning) at a concentration of 10 crypts/μL. The organoids were seeded to 12-well plates, with 70 μL Matrigel:OGM added to each well in 4-5 droplets. The plate was placed in a 37 °C/5% CO_2 incubator for 15 minutes to allow the MatriGel to harden. The MatriGel domes were then immersed in 1 mL OGM and returned to the 37 °C/5% CO_2 incubator. OGM was changed every 3-4 days, and the organoids were passaged once every 5-7 days.

R553X correction in intestinal organoids using LNP-ABE

Organoids were grown in Matrigel droplets in a 12 well plate to approximately 75% confluency with Mouse Intesticult OGM containing 10 μM Y-27632 (STEMCELL Technologies) and 5 μM CHIR 99021 (Sigma-Aldrich). Organoids were released from Matrigel using PBS and centrifugation. Pelleted organoids are resuspended in 1 mL of Acutase (Life Technologies) and incubated at 37 °C for 5 minutes to digest organoids into single cells. Digestion was halted by quenching the Acutase with 2 mL of DMEM media containing 10% FBS. Single stem cells were then placed in an eppedorf tube with 200 μL of OGM containing 0.8 μg of total RNA (*ABE* mRNA:sgR553X=1:1, wt/wt) and incubated at 37 °C/5% CO_2 for 4 hours. Cells and media were then placed in one well of a Matrigel coated 96-well plate. Cells were grown at 37 °C/5% CO_2 for approximately 4-5 days until full organoids develop from the surviving single stem cells. Forskolin-induced swelling of the resulting intestinal organoids were carried out as previously described (*62*, *63*), with small modifications. 200 μL OGM containing 20 μM forskolin was added to each well, creating a 10 μM final concentration. Kinetic brightfield images of FIS were acquired under live cell conditions with a Lionheart FX Automated Microscope (Biotek Instruments, Winooski, Vermont). After one hour of FIS, each organoid was scored as either corrected for CFTR activity, if the organoid swelled, or not corrected for CFTR activity, if the organoid did not swell. Eight 96 wells per treatment group were used for each experiment. DNA was isolated from each well for sequencing of the R553X locus.

Sanger sequencing analysis

Passive Cell lysis Buffer (Promega, Cat# E1941) with proteinase K (Thermal Fisher, Cat# EO0492) was used according to the manufacturer's recommendations to isolate genomic DNA of 16HBEge cells, $CFTR^{R553X/F508del}$ HBE cells through a PCR program (65 °C for 15 min, 95 °C for 10 min). R553X target sequence was amplified using KAPA polymerase (Roche, Cat# 50-196-5243) with the primers listed in **Table S3** following s PCR program (95 °C for 5 min; (95 °C for 30 s; 63 °C for 30 s; 72 °C for 30 s) for 35 cycles; 72 °C for 7 min and then keep at 4 °C). 40 ng of gDNA from intestinal organoids derived from R553X homozygous mice was used for the PCR reaction using a Phusion U Green Multiple PCR Master Mix (Thermo Fisher, Cat# F564S) with an amplification program (98 °C for 3 min; (98°C for 10 s; 58°C for 30 s; 72°C for 30 s) for 30 cycles; 72°C for 2 min). The PCR products were purified using Qiagen PCR purification kit (Qiagen, Cat# 28106), then sequenced by the McDermott Center Sequencing core facility at UTSW. The editing efficiency was determined by analyzing the Sanger sequencing results with EditR (http://baseeditr.com/) (*58*).

Targeted amplicon deep sequencing analysis

Deep amplicon sequencing was used to measure the on-target base editing efficiency in P3 $CFTR^{R553X/F508del}$ HBE culture and lungs from compound heterozygous R553X mice carrying human exon 12 containing the R553X mutation treated with LNP-ABE. Lung single cells were isolated from the snap frozen R553X mice, then $NGFR^+$ cells from bulk lung single cells were isolated from using magnetic cell separation as previously described. Genomic DNA was isolated from lung single cells and $NGFR^+$ cell from the bulk lung using NucleoSpin Tissue XS kits (MACHEREY-NAGEL, Cat# 740901.50). The on-target site for human R553X sequence was PCR amplified with primers listed in the supplementary **Table S3** with the addition of 8 bp barcodes on both ends. 40 ng of gDNA was used for the PCR reaction using a Phusion U Green Multiple PCR Master Mix (Thermo Fisher, Cat# F564S) with an amplification program (98 °C for 3 min; (98 °C for 10 s; 58 °C [R553X mouse]/63 °C [R553X HBE] for 30 s; 72 °C for 30 s) for 30 cycles; 72 °C for 2 min). PCR products were purified with Qiagen PCR purification kit (Qiagen, Cat# 28106) with 25 μL of DNase free water and quantified by Qubit dsDNA high-sensitivity assay (Invitrogen, Cat# Q33231). Targeted amplicon deep-sequencing library was then prepared and later sequenced by Novogene using Illumina NovaSeq 6000. After demultiplexing, amplicon sequencing data were analyzed with CRISPResso2 (https://crispresso.pinellolab.partners.org/) to determine the editing efficiency (*59*).

Display items

The images of lipid nanoparticles, human, mice, lungs, syringes, cells, proteins, plates, and pipettes (Figs. 1A, 1B, 3A, 3I, 3N and Supplementary figs. 3A, 5A, 7A, 12A, 14A, 14D) were created with BioRender.com.

Statistical analyses

Statistical analyses were performed using Prism 9 (GraphPad Software, version 9.5.1). Data are presented as individual data points or mean +/- standard error of the mean (SEM). Statistical tests were performed in GraphPad Prism 9. A two-tailed unpaired t-test was used for comparison between the respective two groups, one-way ANOVA was used for comparison between three or more groups with one variable. P values less than 0.05 were considered statistically significant.

Supplementary Text

Additional background on basal cells and markers used in identification and characterization.

Basal cells are considered the tissue-specific stem cells in both mouse and human airway epithelium, given their capacity to self-renew and differentiation into various mature cell lineages including ciliated, secretory, goblet, and ionocytes (*25-28*). Basal cells in the mouse and human airway epithelium can be identified by the expression of nerve growth factor receptor (NGFR) (*28*) or cytoskeletal protein keratin 5 (KRT5) (*29*). Lineage tracing and clonal growth studies have supported their roles in differentiation and regeneration (*26, 28-30*). When isolated, these cells (NGFR+, KRT5+) can grow in Matrigel, forming clonal structures with markers for ciliated and Clara cells (*28*). This growth is supported by a medium with EGF, FGF, and bovine pituitary extract. Lineage tracing studies in mice using a CK5–CreER model show KRT5-positive basal cells developing into ciliated cells in the proximal airways under normal and post-sulfur dioxide injury conditions (*26, 28*). More recently, KRT5-positive stem cells from bronchiolar regions have been observed to repair alveolar lung tissue post H1N1 infection, forming organized, spherical "pods" and expressing alveolar-specific proteins (*29, 30*).

Additional information regarding Lung SORT LNP mediated CRISPR-Cas9 editing in the lungs.

Ai14 tdTomato reporter mice were analyzed following IV administration of Lung SORT LNPs encapsulating *Cas9* mRNA and sgTOM1 (*32*) (2:1, wt:wt) (**Table S1**) (LNP-Cas9) (2 mg/kg per dose, 3 doses 7 days apart). LNP-Cas9 mediated in vivo editing yielded persistent tdTom expression across the lungs through the eight-month end point including >16% in whole lung cells, >40% in endothelial cells, >7% in immune cells, >25% in epithelial cells, >10% in stem cells (**Fig. S3**). In addition, analysis of lung immune cell types demonstrated that 22.6% of neutrophils, 41.7% of macrophages, 32.4 dendritic cells, 14.9% B cells, 14.9 $CD4^+$ T cells and 13.5% $CD8^+$ T cells were successfully edited (**Fig. S7**)

Additional information on VtnR expression in mouse tissues.

Previous work from other groups demonstrated preferential vascular expression of the vitronectin receptor (VtnR) in the lungs compared to the beds of other organs including the liver and the kidneys (*77*). Our data confirmed that the lung is the most VtnR enriched organ (24.4%) among all tested organs (<4%) (**Fig. S17A**). In non-endothelial cell populations, tdTom expression was enriched within the $VtnR^+$ fraction in heart (24.8% vs 2.9%), lung (23.3% vs 2.9%), liver (88.3% vs 52.4%), spleen (10.4% vs 4.6%), and kidney (24.6% vs 2.7%) (**Fig. S17C**) following LNP-Cre delivery.

Additional information on immune cell editing for CF.

CF is associated with neutrophil abnormality (*33*) and macrophage dysfunction (*34*), causing chronic airway inflammation and a progressive decline in lung function. As noted in the **Main Text**, we performed flow cytometry analysis of a comprehensive immune cell panel, revealing that 22.6% of neutrophils, 41.7% of macrophages, 32.4% of dendritic cells, 14.9% of B cells, 14.9%

of $CD4^+$ T cells, and 13.5% of $CD8^+$ T cells were transfected by LNP-Cre in mouse lungs at tested dose (**Fig. S7**). Editing was also achieved in lung immune progenitor cells (**Fig. S17**).

Additional background on the HBE assay.

Unlike non-CF derived HBE cultures, fully differentiated CF HBE cultures display similar function characteristics associated with CF airway phenotype in vivo, including accumulation of thick sticky mucus and abnormal ion and fluid transport (*54*) . By measuring CFTR-dependent current changes, the area under the curve (AUC) between forskolin and ivacaftor (VX-770) stimulation, one can quantify the functional restoration of CFTR. In this study, we used primary HBE culture carrying compound heterozygous mutations, one allele with R553X mutation and the other one with F508del mutation. Therefore, the baseline editing level of C% on the target position in untreated control is 50% (from the F508del allele). As noted in the **Main Text**, CFTR modulator Trikafta (elexacaftor/tezacaftor/ivacaftor, standard-of-care for CF persons with at least one F508del allele, or any of the other approved mutations (*60*)) was used to compare the therapeutic efficacy of LNP-ABE.

Additional information on the comparison of SORT LNP delivery to differentiated HBEs by basolateral and apical administration.

Additionally, we assessed the transfection efficiency of SORT LNPs delivering tdTomato mRNA (LNP-tdTom) in fully differentiated human bronchial epithelial (HBE) cells on trans-wells through basolateral administration (**Fig. S20**) to mimic in vivo systemic delivery to the lungs, as LNPs can reach the lung stem cells and mature epithelium through intravenous administration (IV) from blood side. Flow cytometry analysis showed that over 50% of basal cells, 36.8% of club cells, and 9.5% ciliated cells. were transfected from the basolateral side.

Additional information on the functional organoid model.

In the forskolin-induced swelling (FIS) assay (*62, 63*), forskolin activates CFTR, stimulates intracellular pathways, and phosphorylates CFTR to open the CFTR channel, permitting ion/water uptake and ultimately organoid swelling. Once the mutated CFTR gene is corrected, organoid swelling should be observed, while untreated organoids will remain at the baseline volume (**Fig. 3J, Movie S4**).

Additional information on Vitronectin-bound SORT LNP delivery.

Vitronectin is a protein secreted into the blood by the liver. Following intravenous administration of the LNPs, an interfacial layer of blood proteins, termed the protein corona, forms around the LNPs. Among the subset of proteins which highly bind to the surface of Lung SORT LNPs is vitronectin (**Fig. S13**). Functionally, vitronectin on the LNP surface may affect which cells can interact and take up the LNPs by binding to its cognate receptors (vitronectin receptor, VtnR) highly expressed by cells within the target organ.

Additional background information on CF gene therapy,

The first gene therapy clinical trial for CF took place in 1993 (*66*). Since then, numerous subsequent trials utilizing various viral vectors took place, but unfortunately there are still no FDA-approved gene therapies in CF. As noted in Main Text, advancement in viral vectors for gene therapy (*66*) and lung delivery (*70, 71*) have continued to be made, with adeno-associated (AAV) virus and lentiviral vectors having been used in clinical trials for CF gene therapy . In one such ongoing clinical trial, AAV-based gene therapy 4D-710 is using an optimized AAV capsid for lung delivery. Due to the limited packaging capability of AAV (~4.6 kb), a transgene encoding human CFTR with a deletion in the regulatory domain [CFTRΔR] was constructed. Previous studies showed that AAV-mediated transgene expression of truncated CFTR leads to functional rescue of CFTR function in well differentiated CF airway epithelia, intestinal organoids, and mouse models (*68, 69*). Besides AAV (*71*), lentiviral vectors also exhibit promise for CF gene therapy because of their larger packaging capability allowing expression of full-length human CFTR, their ability to integrate into the host genome facilitating durable gene expression, as well as their tolerability for repeat dosing. A trial using lentiviral vectors for CF gene therapy is currently in preparation (*67*). These advantages are associated with the risk of gene disruption by unpredictable insertion of exogenous DNA. Collectively, these results highlight potential advantages of systemic delivery of therapeutic genome editors to treat multiple-organ disease, such as CF.

Supplementary Figures

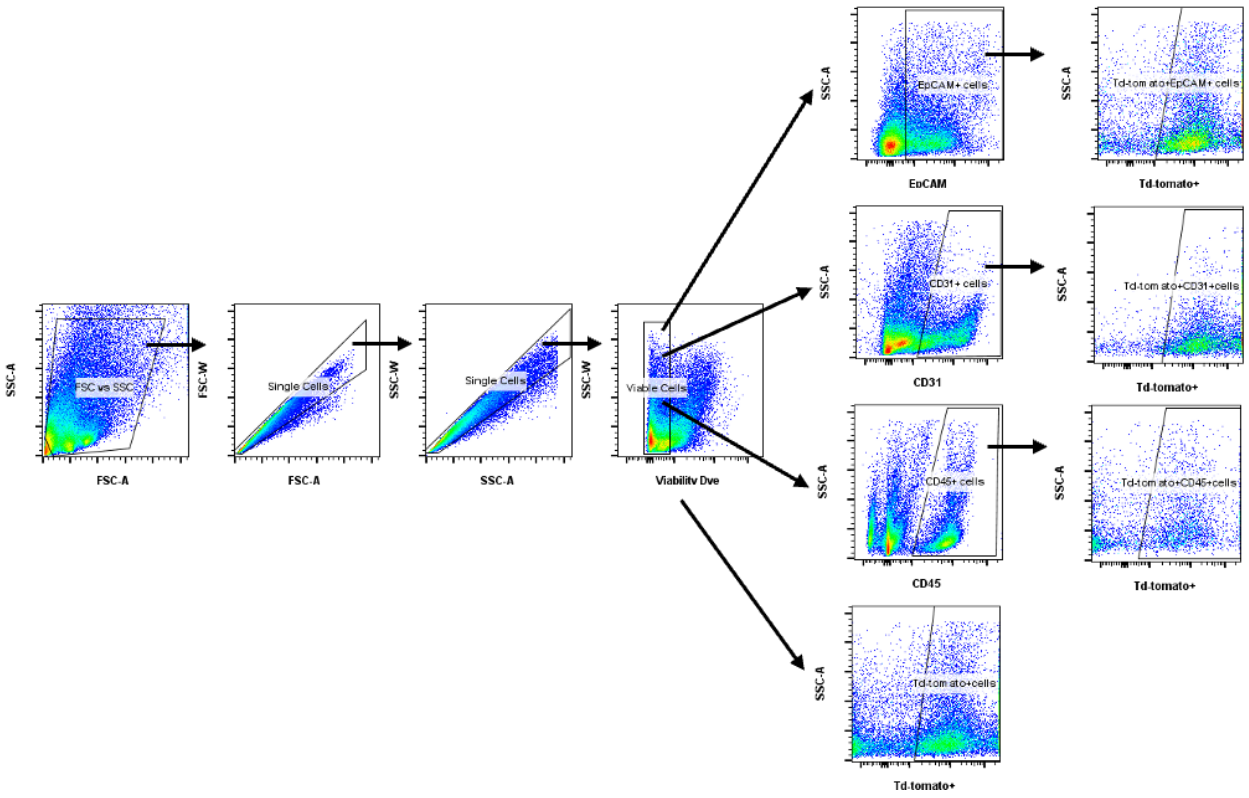

Fig. S1. Flow cytometry gating strategy for lung endothelial, epithelial, and immune cells. Single cells prepared from Ai14 mouse lungs were gated. Viable (Ghost Red negative) total lung cells, endothelial cells (CD31 positive), epithelial cells (EpCAM positive), or immune cells (CD45 positive) expressing tdTomato fluorescence (tdTom positive) were analyzed by flow cytometry (n=3).

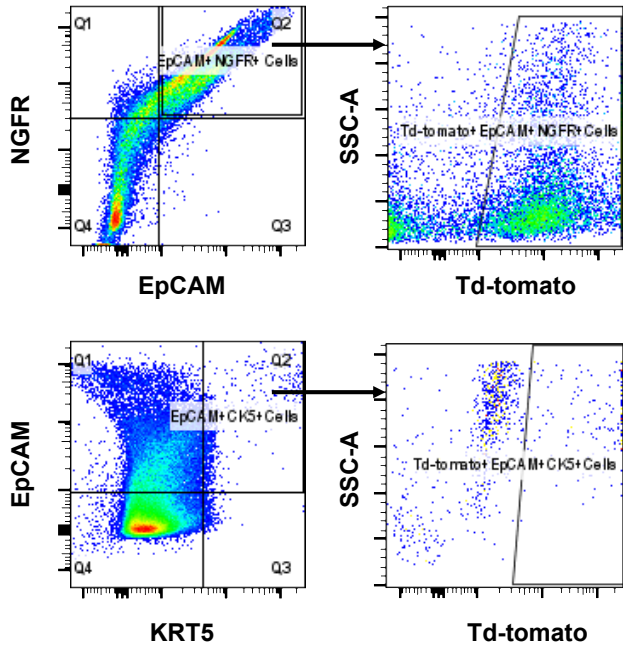

Fig. S2. Flow cytometry gating strategy for lung stem cells. Single cells prepared from Ai14 mouse lungs were gated. Viable (Ghost Red negative) lung stem cells (EpCAM positive, NGFR positive) and lung stem cells (EpCAM positive, KRT5 or CK5 positive) expressing tdTomato fluorescence (tdTom positive) were analyzed by flow cytometry (n=3).

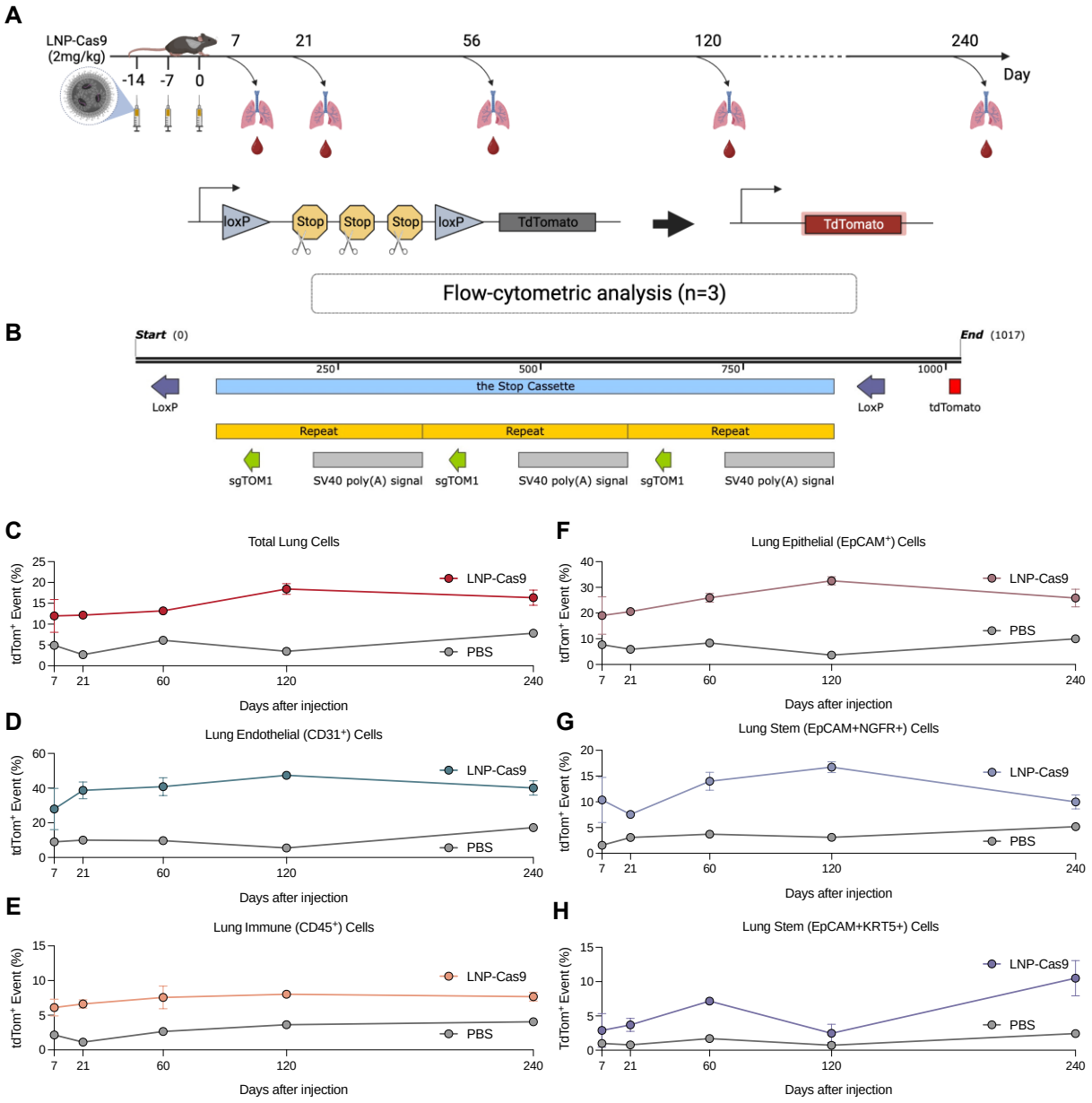

Fig. S3. Durable in vivo gene editing in mouse lung with LNP-Cas9. (**A**) Schematic representation of experimental procedure used to evaluate the efficiency of lung cell editing in Ai14 tdTomato reporter mice, in which Cas9/sgTOM1 can delete the stop cassette enabling tdTomato fluoresce protein expression. (**B**) The location of sgTOM1 on the stop cassette. Lung SORT LNPs were used to co-deliver *Cas9* mRNA and sgTOM1 (LNP-Cas9). Mice were intravenously injected with LNP-Cas9 at 2 mg/kg total RNA (*Cas9* mRNA: sgTOM1=2:1, wt/wt; total lipid to total RNA=20:1, wt/wt) with three sequential doses, one week apart. Mice treated with PBS was used as negative control. Time-course flow cytometry analyses 7, 21, 60, and 240 days after the last injection showing the percentage of tdTomato-positivie ($tdTom^+$) cell was reported among (**C**) total lung cells, (**D**) lung endothelial cells, (**E**) lung immune cells, (**F**) lung epithelial cells, (**G**) $NGFR^+$ lung stem cells, and (**H**) $KRT5^+$lung stem cells. Similar to the result of Cre editing, $tdTom^+$ cells retained persistent expression across the lungs including 38.7% of

endothelial cells, 32.5% of epithelial cells, 6.1% of immune cells, 16.7% of NGFR^{+} lung stem cells, and 7.2% of KRT5^{+} lung stem cells for up to 240 days. Data are presented as individual data points or mean +/- SEM, (n = 3 biologically independent replicates).

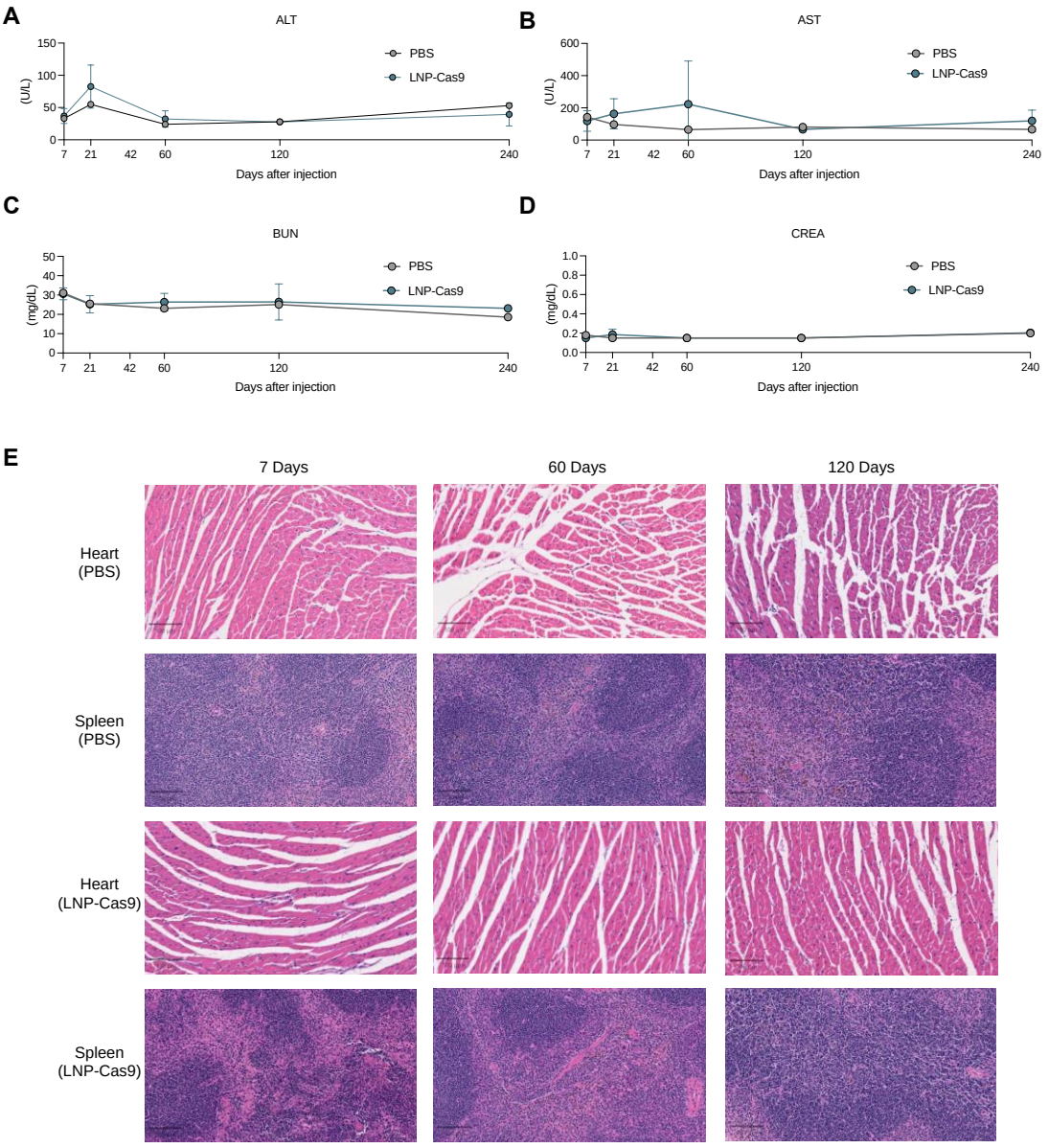

Fig. S4. Minimal toxicity observed after LNP-Cas9 treatments. *In vivo* toxicity of Lung SORT LNPs were evaluated by measuring liver function parameters, ALT (A) and AST (**B**) and kidney function parameters, BUN (**C**) and CREA (**D**) in mouse serum 7, 21, 60, 120, and 240 days after three sequential doses of LNP-Cas9, one week apart (2 mg/kg total RNA, i.v., total lipid/total RNA=20:1) (n = 3 biologically independent replicates). PBS-treated mice were used as a negative control. Data are presented as individual data points or mean +/- SEM. (**E)** Histopathology evaluation was performed by H&E staining of heart and spleen tissues 7, 60, and 120 days after LNP-Cas9 treatment. PBS-treated mice were used as a negative control. Scale bar: 100 µm.

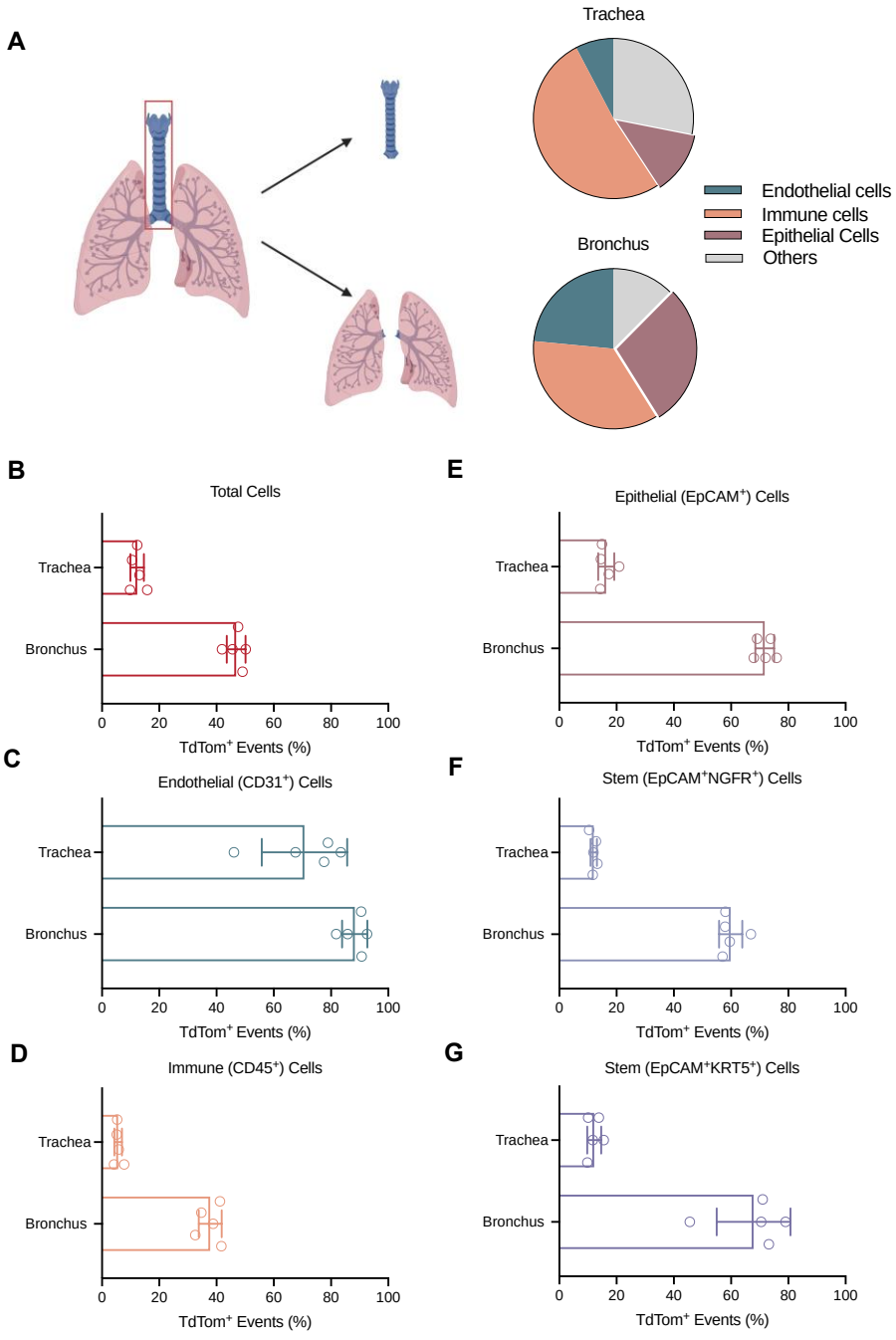

Fig. S5. Lung SORT LNP-mediated editing in tracheal and bronchus regions. To examine whether Lung SORT LNPs facilitate mRNA delivery to the tracheal region of the lung and enable cell editing, LNP-Cre were intravenously administered to Ai14 mice in two successive doses, each being 2 mg/kg total RNA, 48 hours apart. (**A**) The tracheas and bronchus regions were extracted 48 hours following the final injection, and tdTom expression (tdTom$^+$) across various cell types was quantified using flow cytometry. The composition of cells markedly differed between the trachea and bronchus regions of the lung. The trachea harbored more immune cells (55.8%) and fewer epithelial (13.7%) and endothelial cells (8.4%) compared to the bronchus (35.4% immune

cells, 28.7% epithelial cells, and 23.5% endothelial cells). Percentages of total edited cells (**B**), endothelial cells (**C**), immune cells (**D**), epithelial cells (**E**), NGFR$^+$ stem cells (**F**), and KRT5$^+$ stem cells (**G**) in the trachea compared to the bronchus region. Data are presented as mean +/- SEM in **B**-**G** (n = 5 biologically independent replicates).

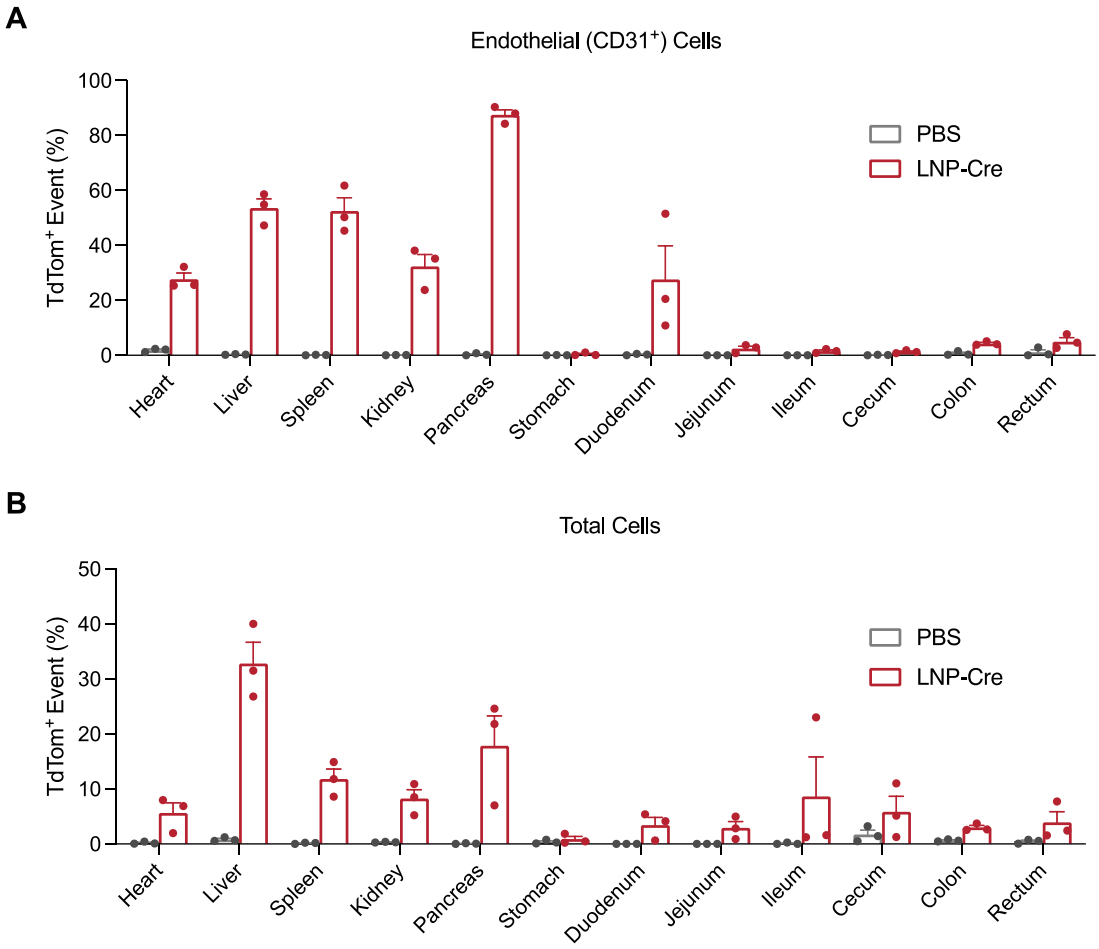

Fig. S6. Gene editing in endothelial beds of various organs with LNP-Cre. LNP-Cre was intravenously administered to Ai14 mice in two successive doses, 2 mg/kg total RNA, 48 hours apart. tdTom expression (tdTom$^+$) across CD31$^+$ endothelial beds of various organs (**A**) and total cells of various organs (**B**) were quantified by flow cytometry. Tested organs include heart, lung, liver, spleen, kidney, pancreas, stomach, duodenum, jejunum, ileum, cecum, colon, and rectum. PBS-treated mice were used as negative control. Data are presented as mean +/- SEM (n = 3 independent replicates).

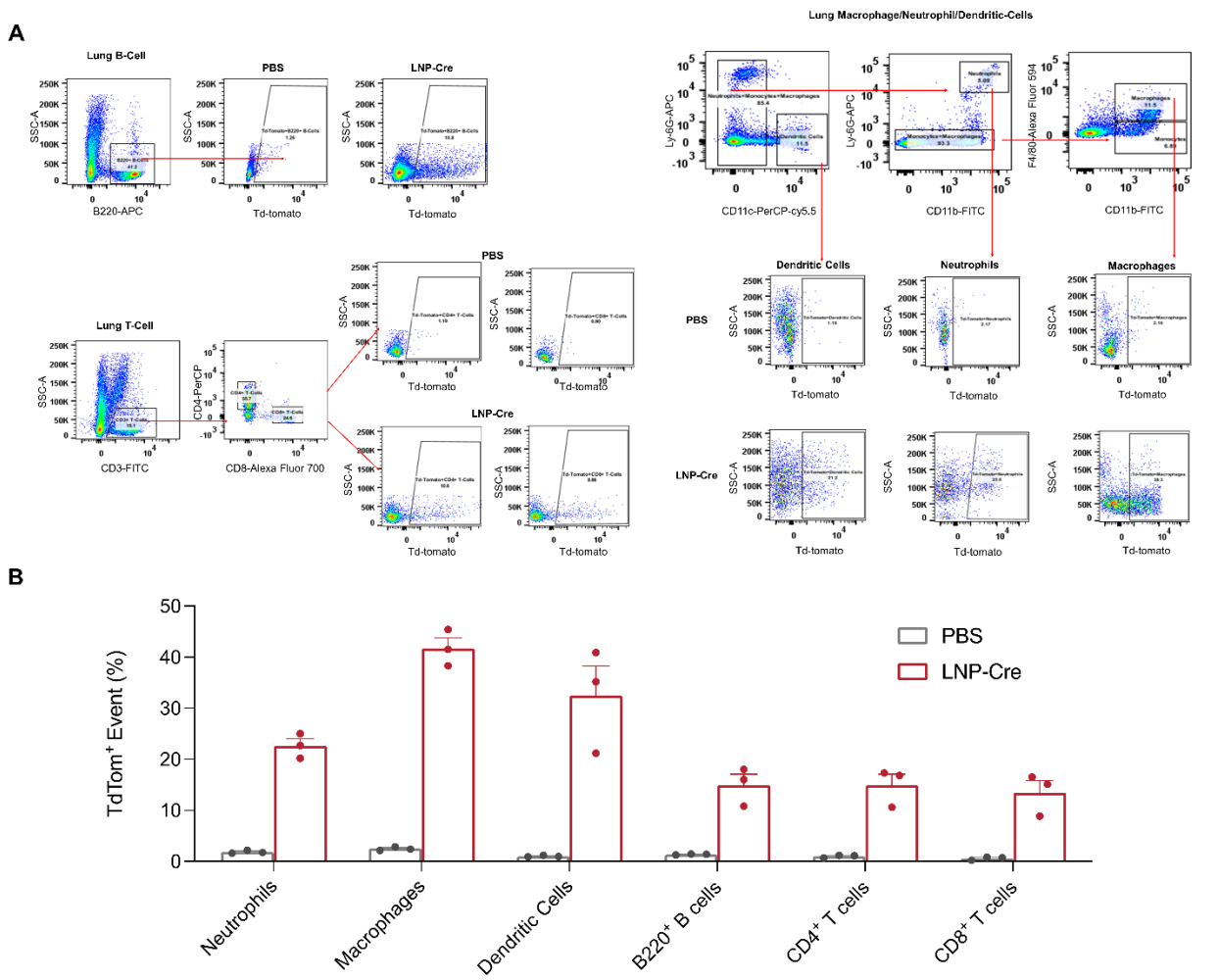

Fig. S7. Lung SORT LNP-mediated editing in lung immune cells. To study whether Lung SORT LNPs facilitate efficient mRNA delivery to various lung immune cells, LNP-Cre were intravenously administered to Ai14 mice in two successive doses, each being 2 mg/kg total RNA, 48 hours apart. (**A**) Flow cytometry gating strategy for various lung immune cells. Single cells prepared from Ai14 mouse lungs were gated. Viable (Ghost Red negative) lung immune cells (CD45 positive) including B cells (B220 positive), CD4 T cells (CD3 positive CD4 positive), CD8 T cells (CD3 positive CD8 positive), dendritic cells (CD11c positive), neutrophils (Ly-6G positive) and macrophages (F4/80 positive) were analyzed by flow cytometry to evaluate tdTomato expression level (tdTomato positive). PBS treated mice were served as negative control. (**B**) The results showed that 22.6% of neutrophils, 41.7% of macrophage, 32.4% of dendritic cells, 14.9% B cells, 14.9% $CD4^+$ T cells and 14.5% of $CD8^+$ T cells were edited. Data are presented as mean +/- SEM (n=3 biologically independent replicates).

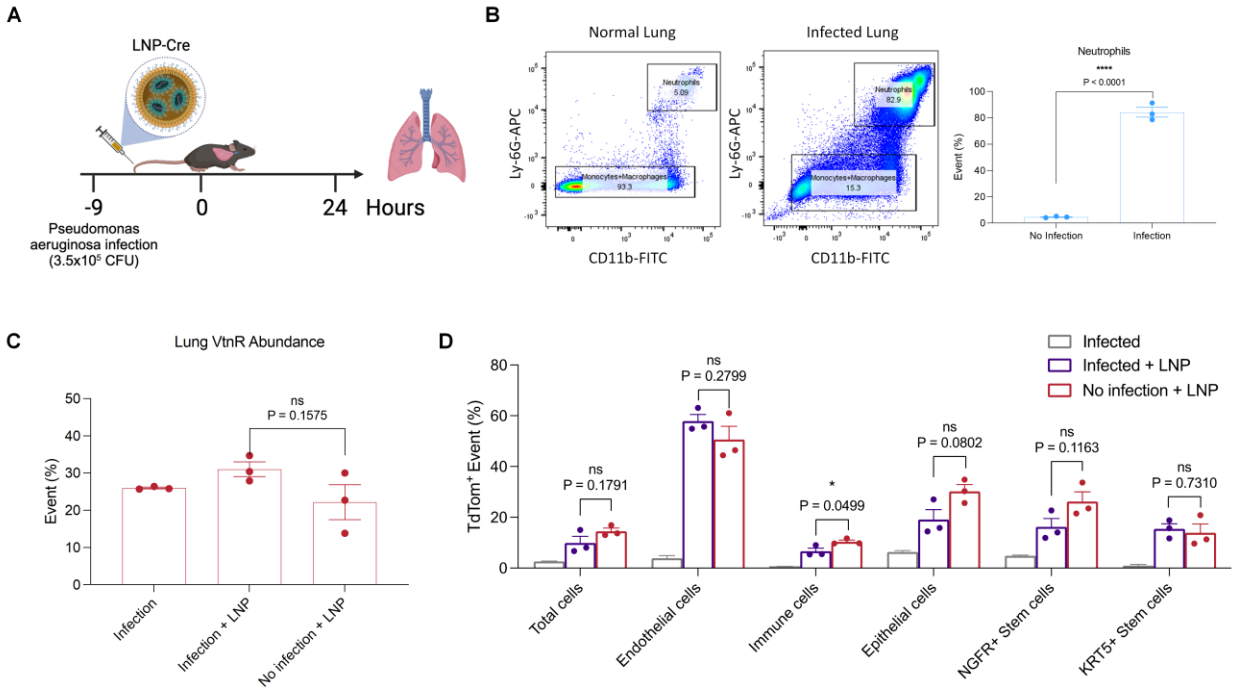

Fig. S8. Lung SORT LNP-mediated editing in P. aeruginosa infected mouse lungs. To examine whether Lung SORT LNPs retain high delivery efficacy in infected and inflamed lungs, Ai14 mice were randomly allocated to P. aeruginosa infection group or non-infection group. (**A**) Mice in infection group were inoculated intranasally with 50 µl of P. aeruginosa at 3.5 x 105 CFU to generate acute infection model. LNP-Cre were intravenously administered to Ai14 mice, 2 mg/kg total RNA, 9 h post infection. Neutrophil invasion was observed in infected lungs 9 h after the intranasal infection compared to non-infected lungs (**B**). VtnR abundance (**C**) and tdTom expression ($tdTom^+$) across various cell types in infected and non-infected mouse lung (**D**) were measured using flow cytometry. No significant difference was observed in VtnR abundance and editing efficiency among various tested lung cell types except immune cells between infected and non-infected lungs. PBS-treated infected mice were used as negative control. Data are presented as mean +/- SEM (n = 3 independent replicates), Unpaired t-test. P values < 0.05 were considered statistically significant.

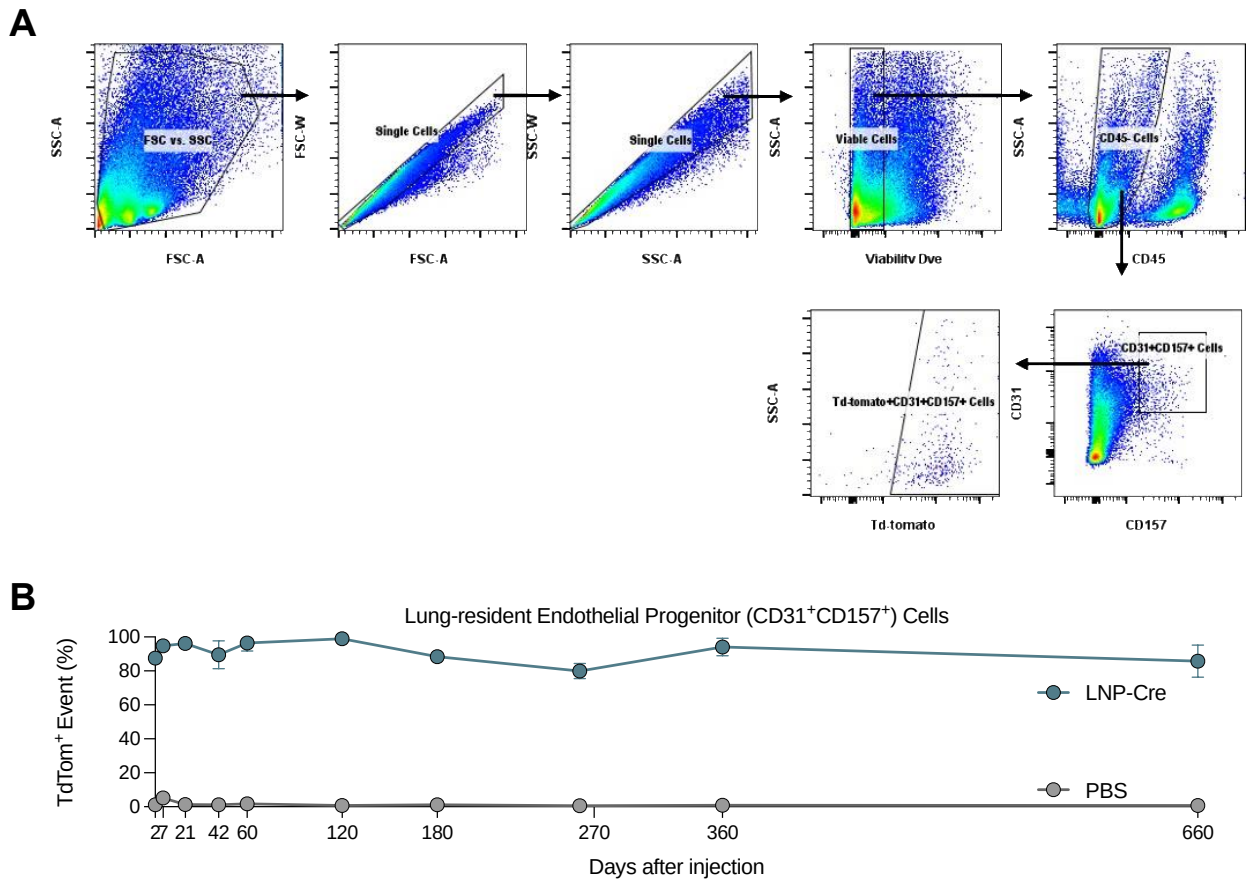

Fig. S9. Gene editing in mouse lung endothelial progenitor cells with LNP-Cre. Ai14 mice were dosed with two sequential LNP-Cre treatments (two days apart) at 2 mg/kg total RNA (20:1, total lipid to RNA weight ratio). The lungs were collected at 2, 7, 21, 42, 60, 120, 180, 270, 360, and 660 days after the last injection. (**A**) Flow cytometry gating strategy for lung endothelial progenitor cells. Single cells prepared from Ai14 mouse lungs inclusive of tracheas were gated. Single cells prepared from Ai14 mouse lungs were gated. Viable (Ghost Red negative) lung endothelial progenitor cells (CD45 negative, CD31 positive, CD157 positive) expressing tdTomato fluorescence (tdTomato positive) were analyzed by flow cytometry. (**B**) Gene editing in mouse lung hematopoietic lung endothelial progenitor cells were obtained from three mice per each time point. PBS treated mice were served as negative control. Data are presented as individual data points or mean +/- SEM (n=3 biologically independent replicates).

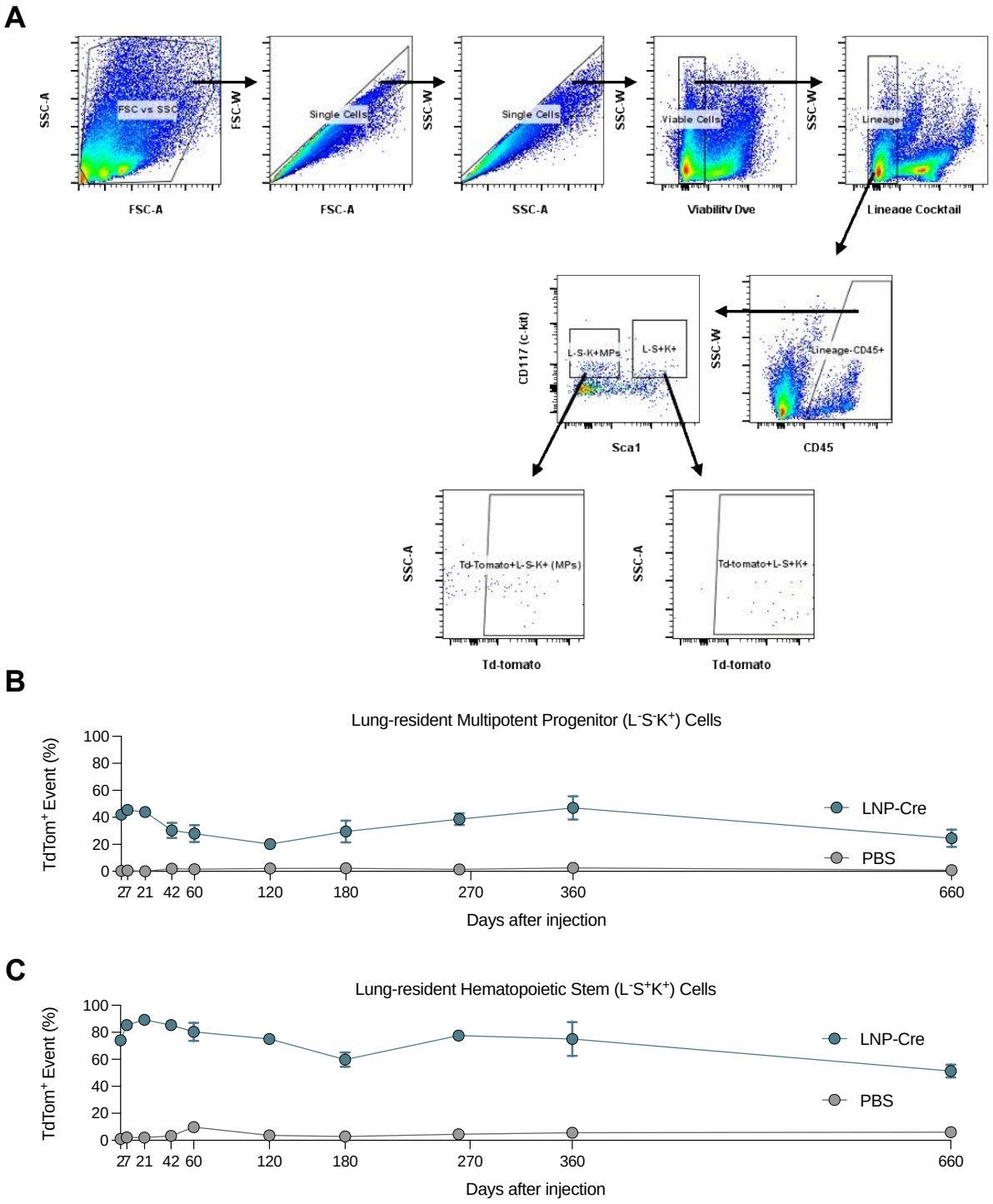

Fig. S10. Gene editing in mouse lung hematopoietic progenitor cells with LNP-Cre. Ai14 mice were dosed with two sequential LNP-Cre treatments (two days apart) at 2 mg/kg total RNA (20:1, total lipid to RNA weight ratio). The lungs inclusive of tracheas were collected at 2, 7, 21, 42, 60, 120, 180, 270, 360, and 660 days after the last injection. (**A**) Flow cytometry gating strategy for lung hematopoietic progenitor cells. Single cells prepared from Ai14 mouse lungs were gated. Viable (Ghost Red negative) lung multipotent progenitor cells (lineage negative, CD45 positive,

Sca1 negative, c-kit positive) or lung hematopoietic stem cells (lineage negative, CD45 positive, Sca1 positive, c-kit positive) expressing tdTomato fluorescence (tdTomato positive) were analyzed by flow cytometry. Gene editing in mouse lung hematopoietic lung multipotent progenitor cells (**B**) and lung hematopoietic stem cells (**C**) were obtained from three mice per each time point. PBS treated mice were served as negative control. Data are presented as individual data points or mean +/- SEM (n=3 biologically independent replicates).

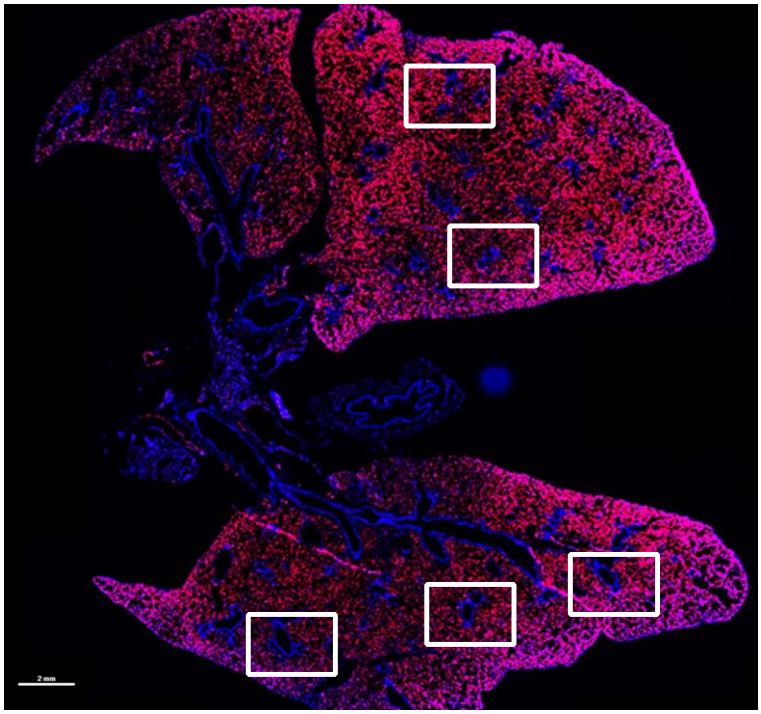

Fig. S11. Representative whole slide images showing five to six random segments selection for quantification analysis.

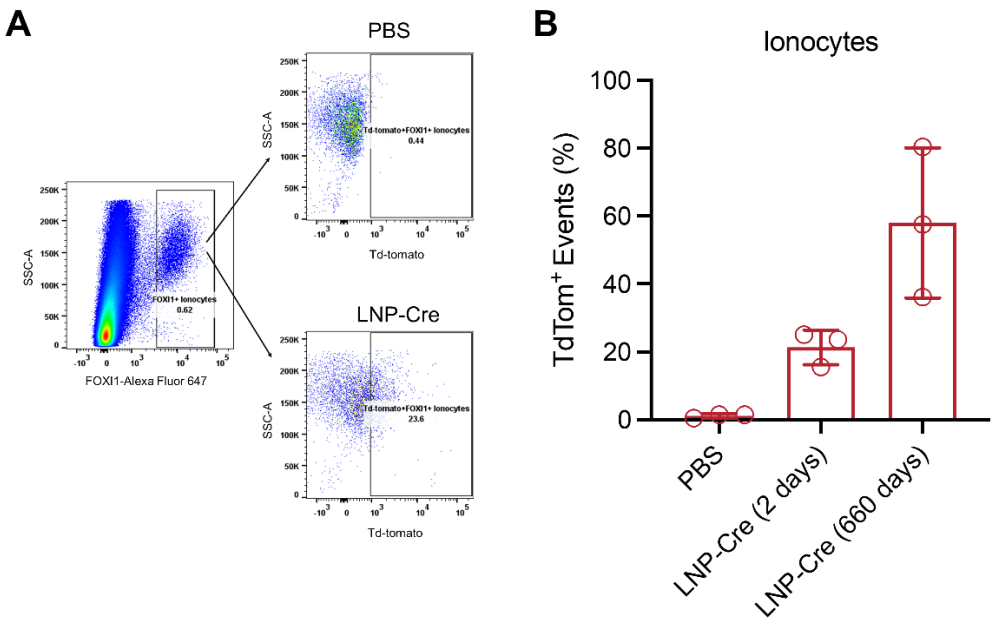

Fig. S12. Gene editing and persistence of gene editing in mouse lung ionocytes following systemic LNP-Cre administration. Ai14 mice were dosed with two sequential LNP-Cre treatments (two days apart) at 2 mg/kg total RNA (20:1, total lipid to RNA weight ratio). The lungs were collected 2 days and 660 days after the last injection. (A) Flow cytometry gating strategy for lung ionocytes. (**A**) FOXI1 positive lung ionocytes were gated and analyzed for the expression of tdtomato fluorescence. (**B**) Editing levels, correlated with tdtomato expression in mouse lung ionocytes, were measured from three mice at each time point. PBS treated mice served as the negative control. Data are presented as mean +/- SEM (n=3 biologically independent replicates).

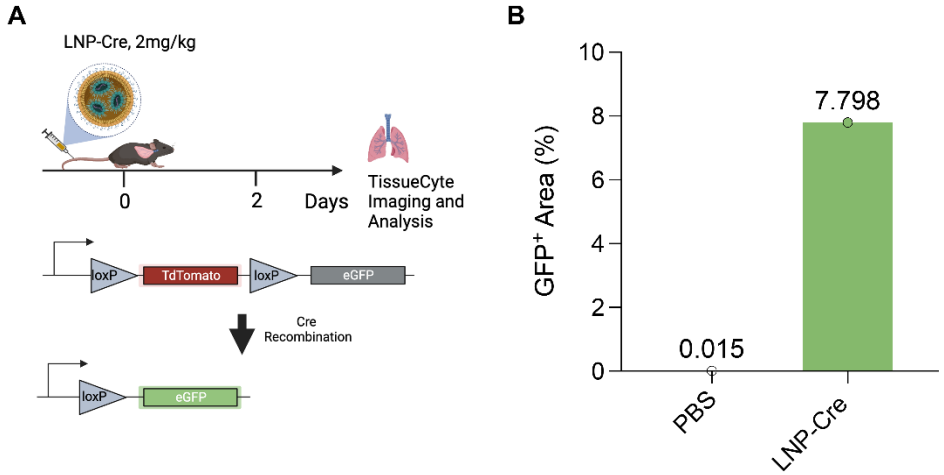

Fig. S13. Quantitative TissueCyte analysis of mTmG mice lung following LNP-Cre treatment. (**A**) Schematic representation of LNP-Cre mediated eGFP fluorescence protein expression replacing the red fluorescence in lung cells after systemic administrations. A mouse was injected intravenously with a single LNP-Cre treatment at 2 mg/kg total RNA (20:1, total lipid to RNA weight ratio). The mouse lung was collected two days after the injection. PBS-treated mTmG mouse was used as negative control. (**B**) Quantitative analysis of GFP positive (GFP^+)

area % in LNP-Cre treated mTmG mouse lung left lobe by TissueCyte 3D imaging and analysis. Data are presented as individual data points (n=1).

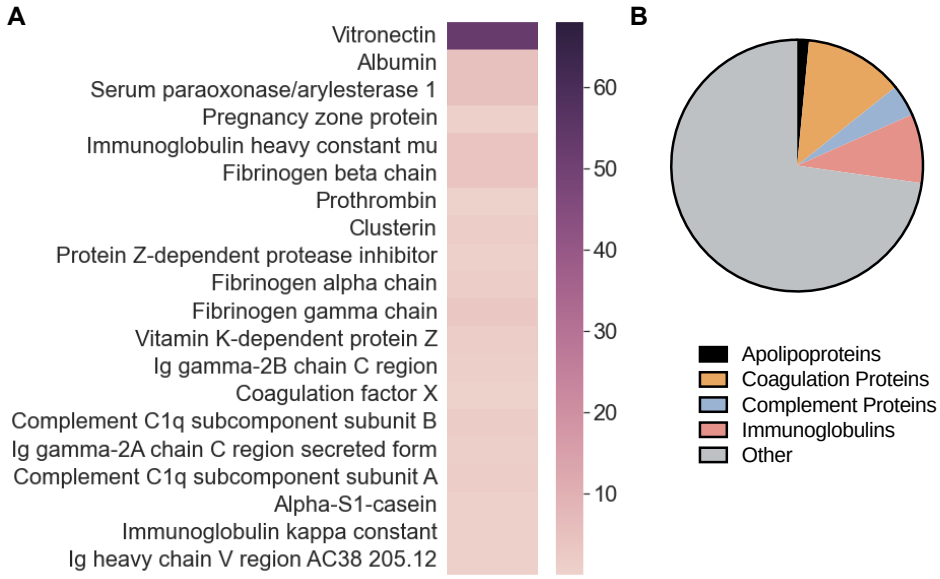

Fig. S14. The protein corona composition adsorbed onto Lung SORT LNP surface determined by unbiased mass spectrometry proteomics. The most abundant proteins were ranked and plotted as a heat map (**A**) and classified into physiological classes of the identified proteins (**B**).

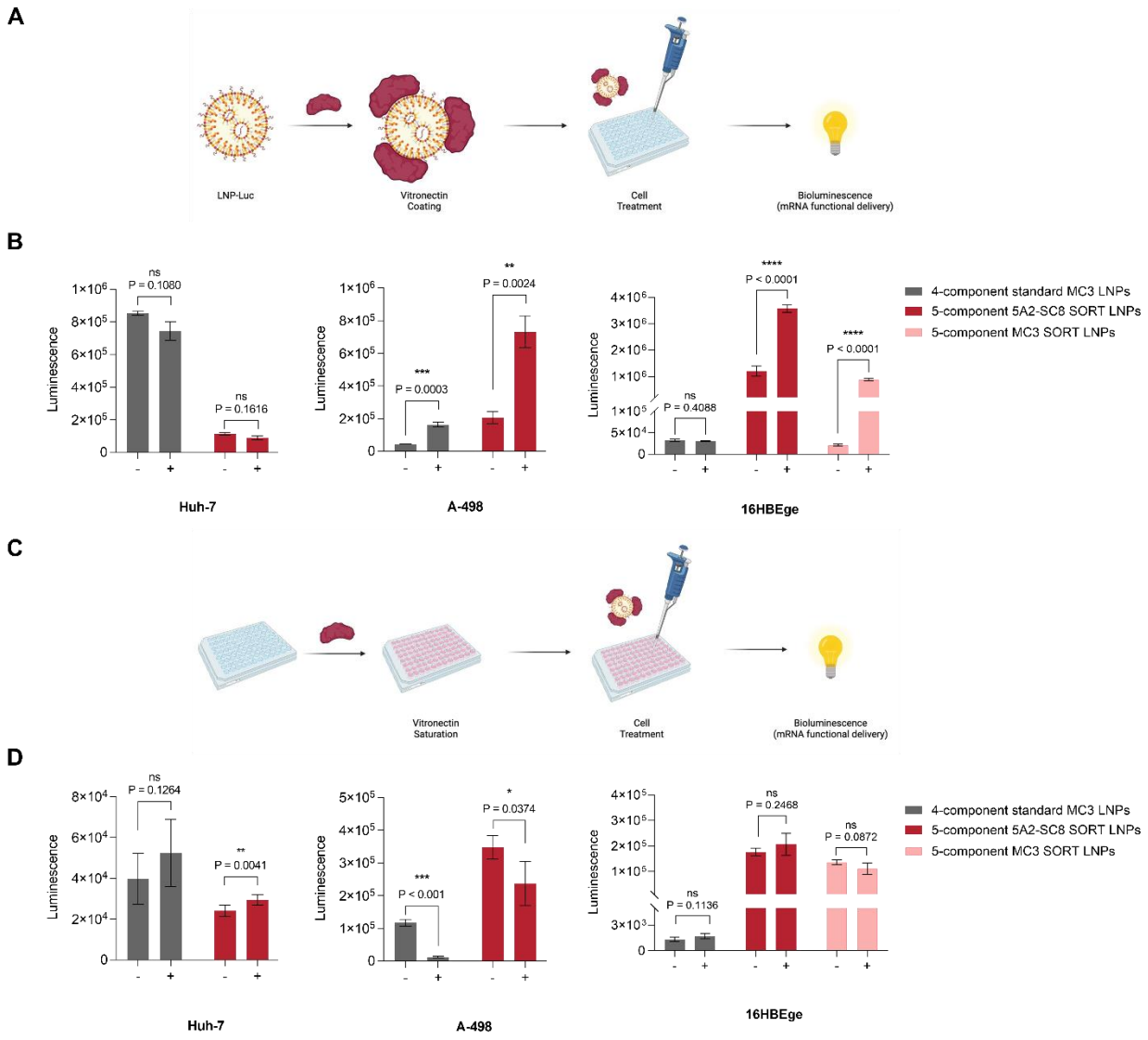

Fig. S15. Vitronectin regulates SORT and non-SORT LNP efficacy in vitronectin receptor (VtnR) expressing cells in vitro. (**A**) 5-component 5A2-SC8 SORT LNPs, 5-component DLin-MC3-DMA (MC3) SORT LNPs, and 4-component non-SORT LNPs (standard MC3 LNPs) were preincubated with 0.25 g Vtn/g lipid prior to treating Vtn-negative liver cancer cells (Huh-7), Vtn-expressing kidney cancer cells (A-498), and Vtn-expressing human lung epithelial (16HBE14o-) cells to measure functional mRNA delivery (bioluminescence). (**B**) The activity of functional luciferase translated from mRNA delivered by uncoated LNPs (labeled "-") or Vtn-coated LNPs (labeled "+") in relevant cell lines (25 ng mRNA, 24 h, n = 4). (**C**) Cells were saturated with 0.2 µg Vtn/mL prior to treatment with Vtn-coated SORT and non-SORT LNPs (which do not bind Vtn) to assess functional mRNA delivery (bioluminescence). (**D**) The activity of functional luciferase translated from mRNA delivered by Vtn-coated LNPs in cells with or without Vtn saturation. (25 ng mRNA, 24 h, n = 4). Statistical significance was determined using an unpaired t test. P values < 0.05 were considered statistically significant. Data are shown as mean +/- SEM.

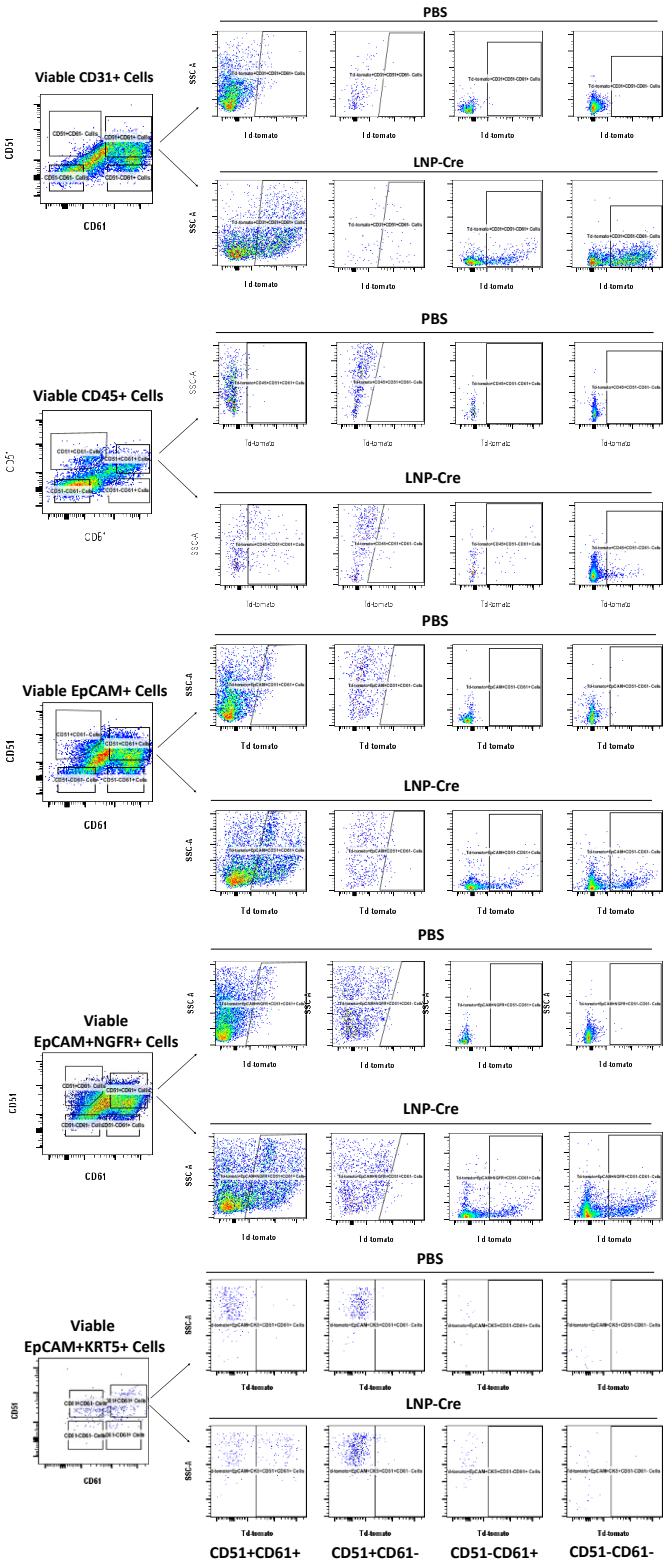

Fig. S16. Flow cytometry gating strategy for vitronectin receptor. Single cells prepared from Ai14 mouse organs were gated. Viable (Ghost Red negative) total cells, vitronectin receptor

expressing (CD51 positive CD61 positive) endothelial cells (CD31 positive), immune cells (CD45 positive), epithelial cells (EpCAM positive), lung stem cells (EpCAM positive NGFR positive or EpCAM positive KRT5 positive) with tdTomato fluorescence (tdTom positive) were analyzed by flow cytometry (n=3).

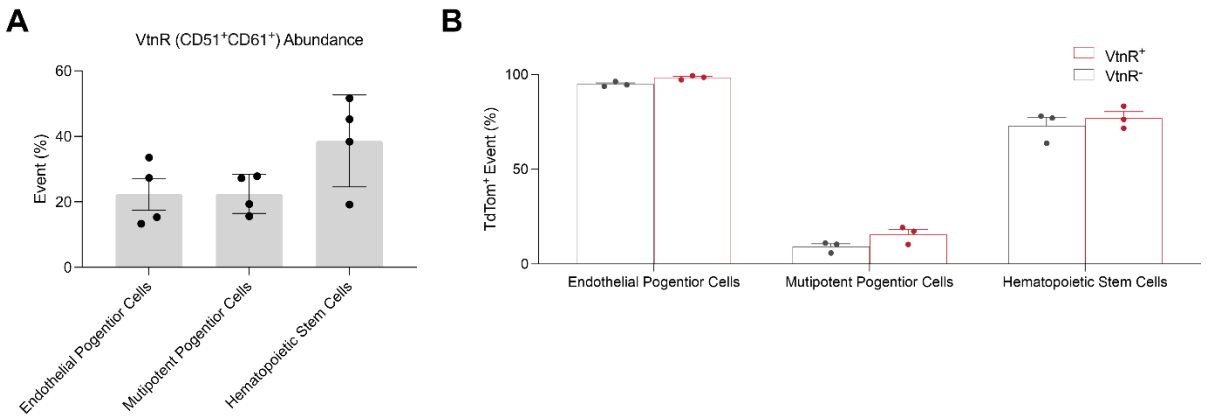

Fig. S17. LNP delivery in VtnR-expressing lung endothelial cells, lung multipotent progenitor cells, and lung hematopoietic stem cells. VtnR ($CD51^+CD61^+$) abundance (**A**) and quantification of tdTom positivity in $VtnR^+$ ($CD51^+CD61^+$) cells and $VtnR^-$ ($CD51^-CD61^-$) fraction in lung endothelial cells, lung multipotent progenitor cells, and lung hematopoietic stem cells (**B**). Ai14 mice were dosed with two sequential LNP-Cre treatments (two days apart) at 2 mg/kg total RNA (20:1, total lipid to RNA weight ratio). The lungs were collected 2 days after the last injection. Single cells prepared from Ai14 mouse lungs were gated. Viable (Ghost Red negative) total lung cells, vitronectin receptor expressing (CD51 positive CD61 positive) endothelial progenitor cells (CD31 positive CD157 positive), lung resident multipotent immune progenitor cells (lineage negative, CD45 positive, Sca1 negative, c-kit positive), or lung resident hematopoietic stem cells (lineage negative, CD45 positive, Sca1 positive, c-kit positive) with tdTomato fluorescence (tdTom positive) were analyzed by flow cytometry. Lung endothelial cells (22.4%), lung multipotent progenitor cells (22.5%), and lung hematopoietic stem cells (38.6%) all exhibit high levels of VtnR expression. Lung SORT LNPs transfect a very high fraction of endothelial and lung hematopoietic stem cells, which may mask any potential contribution of VtnR versus other receptor interactions. Data are mean +/- SEM (n = 3 independent replicates).

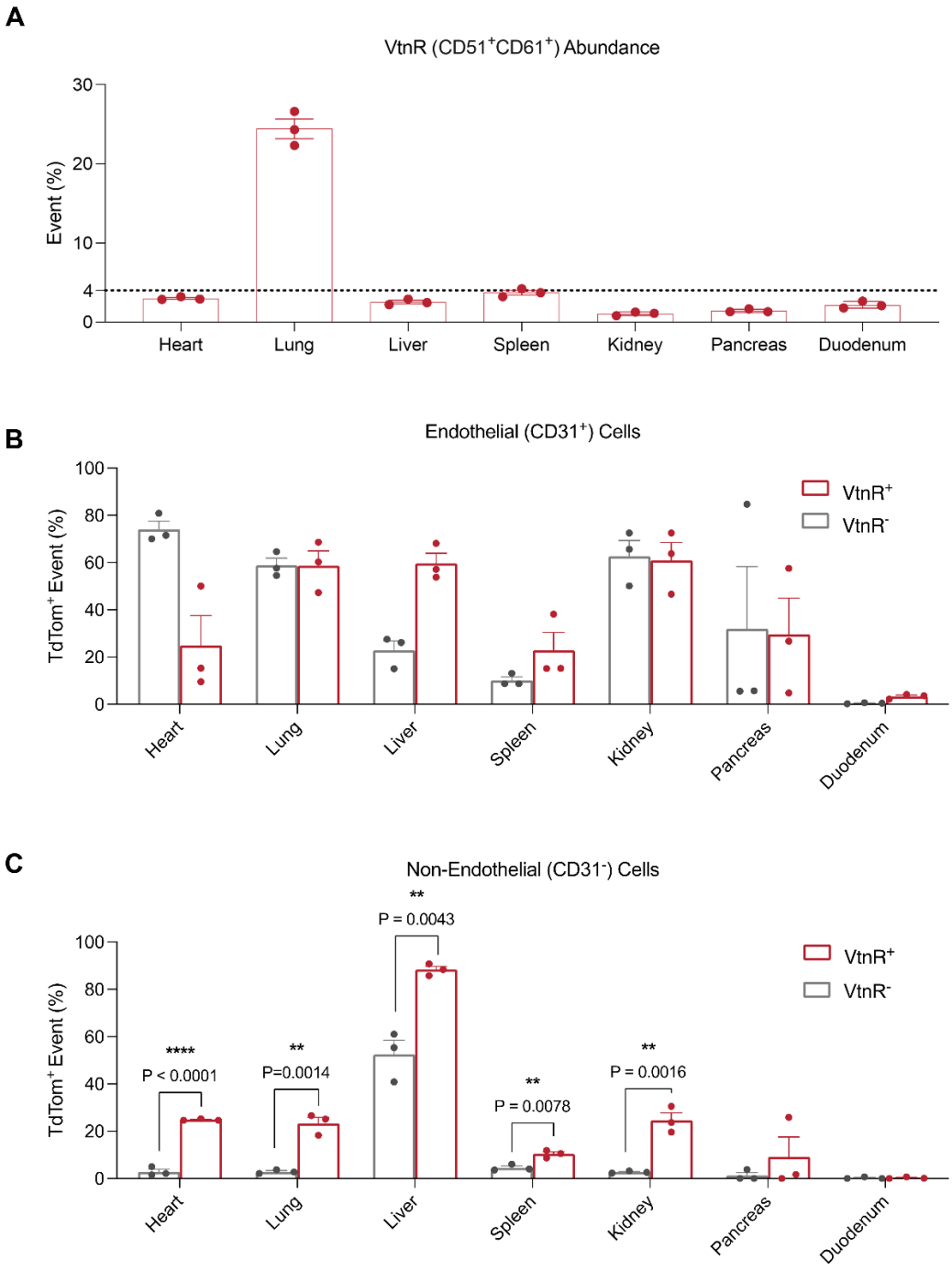

Fig. S18. Profiling of VtnR expression in mouse tissues and LNP delivery in VtnR-expressing lung endothelial and non-endothelial cells. VtnR ($CD51^+CD61^+$) abundance (**A**) and quantification of tdTom positivity in $VtnR^+$ ($CD51^+CD61^+$) cells and $VtnR^-$ ($CD51^-CD61^-$) fraction in endothelial cells (**B**) or non-endothelial cells (**C**) across various organs. Ai14 mice were dosed with two sequential LNP-Cre treatments (two days apart) at 2 mg/kg total RNA (20:1, total lipid to RNA weight ratio). Organs were collected 2 days after the last injection. Single cells prepared from Ai14 mouse organs were gated. Viable (Ghost Red negative) total cells, vitronectin receptor expressing (CD51 positive CD61 positive) endothelial cells (CD31 positive) or non-

endothelial cells (CD31 negative) with tdTomato fluorescence (tdTom positive) were analyzed by flow cytometry. Comparing to heart (3.0%), liver (2.5%), spleen (3.7%), kidney (1.1%), pancreas (1.4%), duodenum (2.2%), ovaries/testes (4.3%), lung exhibit highest level of VtnR expression (24.4%). Endothelial cells of all tested organs displayed no preference for tdTom in $VtnR^+$ or VtnR- fraction. However, in non-endothelial cell population, tdTom expression was enriched within the $VtnR^+$ fraction compared to the $VtnR^-$ fraction in heart (24.8% vs 2.9%), lung (23.3% vs 2.9%), liver (88.8% vs 52.3%), spleen (10.4% vs 4.6%) and kidney (24.6% vs 2.7%). Data are mean ± SEM (n = 3 independent replicates), unpaired t-test. P values < 0.05 were considered statistically significant.

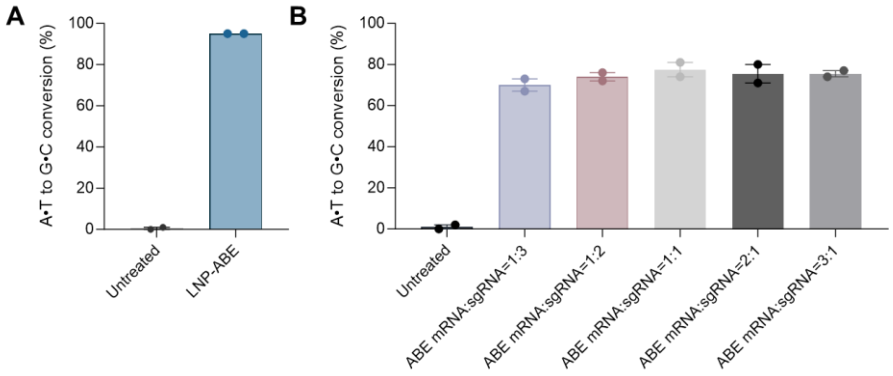

Fig. S19. Efficient adenine base editing in 16HBEge R553X cells. (**A**) LNP-ABE (ABE mRNA:sgR553X=2:1 by weight, 1.5 μg total RNA per well) mediated high level base editing efficiency (>95%) in 16HBEge R553X cells at the target T_7 position. The A•T to G•C conversion on T_7 position was analyzed using EditR analysis with Sanger sequencing data. (**B**) The stoichiometry of ABE mRNA and sgR553X was investigated by measuring the editing level after transfecting 16HBEge cell using a series of LNP-ABE (0.8 μg total RNA per well) with altered ABE mRNA to sgRNA weight ratios. Data are shown as mean +/- SEM (n=2 independent samples).

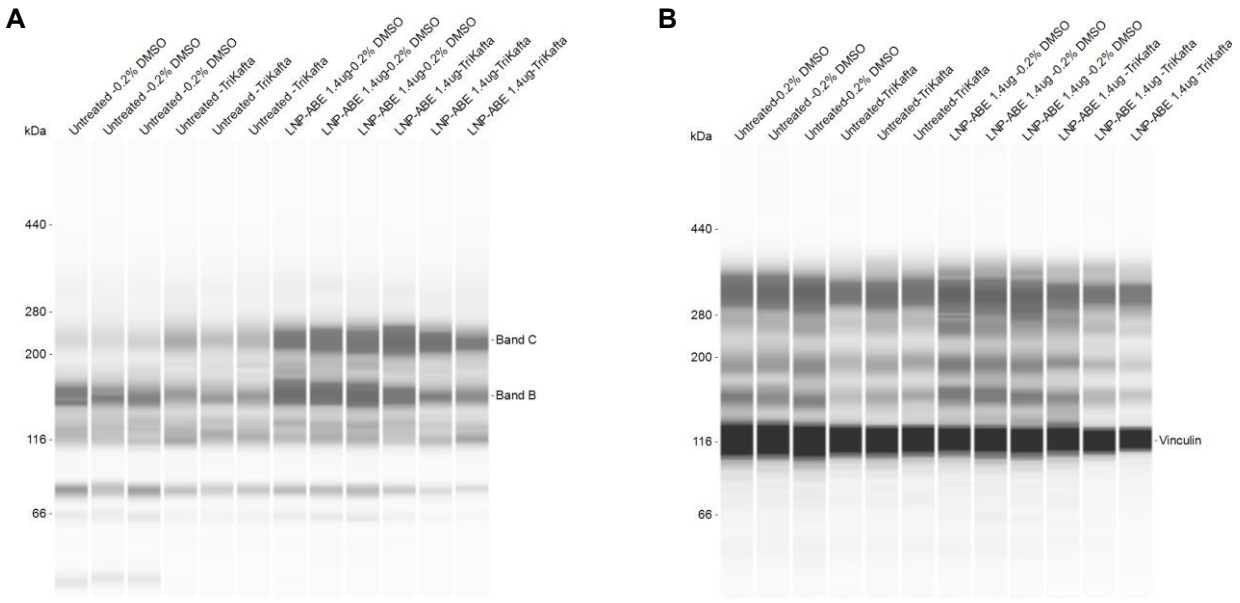

Fig. S20. Raw data of gel images of CFTR (**A**) and Vinculin as internal standard (**B**) from Jess^{TM} capillary western blotting.

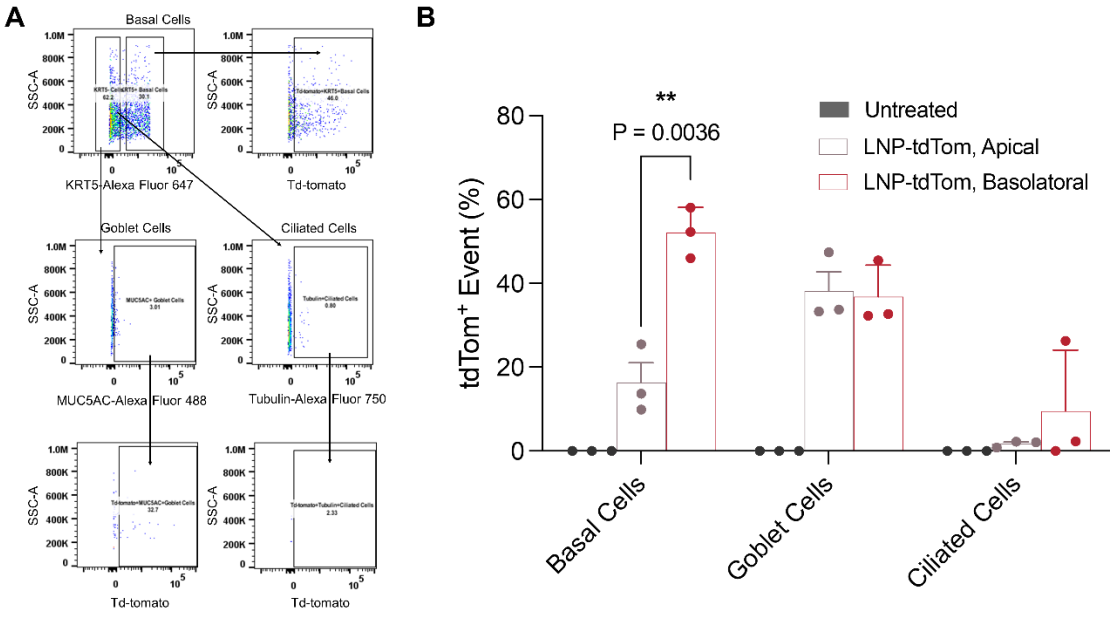

Fig. S21. Apical and basolateral delivery of LNP-tdTom in P3 differentiated HBE R553X/F508del cultures. Cells were then treated with 12 µg LNP-tdTom (12 µg tdTomato mRNA per well) either to the apical side in liquid bolus or to the basolateral side. Untreated HBE cells were used as control. (**A**) Single cells prepared from inserts were gated. Viable (Scarlet 723 negative) basal cells (KRT5 positive), club cells (SCGB1A1 positive), goblet cells (MUC5AC positive), and ciliated cells (Acetyl-Tubulin positive) with tdTomato fluorescence (tdTom positive) were analyzed by flow cytometry. (**B**) Quantitative analysis of tdTom^{+} cells in HBE basal

and differentiated cell populations (n=3). Data are shown as mean +/- SEM. Unpaired t-test. P values < 0.05 were considered statistically significant.

Supplementary Tables

Table S1. Sequences of sgRNA used in this study.

sgRNA	Sequence (5' to 3')	PAM (5' to 3')
sgTOM1	AAGTAAAACCTCTACAAATG	TGG
sgR553X	TTGCTCATTGACCTCCACTC	AG

Table S2. Primary antibody staining conditions used for immunofluorescence.

Cell type	Antibody Name	Vendor	Antibody Catalog #	Primary Antibody Dilution	Primary Antibody Incubation (min)
AT1 cells	Anti-Hop Antibody (E-1): sc-398703	SantaCruz	sc-398703	1:100	20 minutes
AT2 cells	Purified anti-ABCA3 Antibody	Biolegend	911001	1:100	20 minutes
Goblet cells	Recombinant Anti-Mucin 5AC antibody [45M1]	AbCam	ab3649	1:100	20 minutes
Ciliated cells	Monoclonal Anti-Tubulin, Acetylated antibody produced in mouse	Millipore Sigma	T6793-100UL	1:100	20 minutes
Club sells	Anti- SCGB1A1 antibody	AbCam	ab40873	1:100	20 minutes

Table S3. Primers used for sequencing analyses.

Target	Primer	Sequence (5' to 3')
R553X (HBE model)	Forward	GGAAGATGTGCCTTTCAAATTCAG
	Reverse	ATGTGATTCTTAACCCACTAGCCA
R553X (Mice model)	Forward	GGAAGATGTGCCTTTCAAATTCAG
	Reverse	ACAGCAAATGCTTGCTAG

Table S4. Characterization of Lung SORT LNPs encapsuling ABE mRNA/sgR553X made by vortex mixing or T-mixing.

Mixing technique	Particle size (nm)	PDI	Zeta potential	% encapsulation
Vortex mixing	130.0 ± 0.8	0.14 ± 0.01	6.29 ± 0.34	82.9 ± 1.1
T-mixing	90.0 ± 0.7	0.14 ± 0.03	6.28 ± 0.56	98.2 ± 0.0

Captions for Supplementary Movies

Movie S1. 3D Rendering of Ai14 mouse lung after LNP-Cre treatment

Movie S2. 3D Rendering of untreated mTmG mouse lung

Movie S3. 3D Rendering of mTmG mouse lung after LNP-Cre treatment

Movie S4. Untreated **o**rganoids

Movie S5. Organoid swelling after LNP-ABE treatment